Neurochemical Research (2019) 44:1549–1566
https://doi.org/10.1007/s11064-019-02776-7

ORIGINAL PAPER

Intrinsic Effects of Gold Nanoparticles on Oxygen–Glucose Deprivation/Reperfusion Injury in Rat Cortical Neurons

Yafei Zheng[1,3] · Yuyun Wu[1,3] · Ying Liu[1,3] · Zhirui Guo[1,3] · Tingting Bai[1,3] · Ping Zhou[1,3] · Jin Wu[2] · Qin Yang[4] · Zhengxia Liu[1,3,5] · Xiang Lu[1,3,5]

Received: 18 January 2019 / Revised: 8 March 2019 / Accepted: 9 March 2019 / Published online: 15 May 2019

Abstract

This study aimed to investigate the potential effects of gold nanoparticles (Au-NPs) on rat cortical neurons exposed to oxygen–glucose deprivation/reperfusion (OGD/R) and to elucidate the corresponding mechanisms. Primary rat cortical neurons were exposed to OGD/R, which is commonly used in vitro to mimic ischemic injury, and then treated with 5- or 20-nm Au-NPs. We then evaluated cell viability, apoptosis, oxidative stress, and mitochondrial respiration in these neurons. We found that 20-nm Au-NPs increased cell viability, alleviated neuronal apoptosis and oxidative stress, and improved mitochondrial respiration after OGD/R injury, while opposite effects were observed for 5-nm Au-NPs. In terms of the underlying mechanisms, we found that Au-NPs could regulate Akt signaling. Taken together, these results show that 20-nm Au-NPs can protect primary cortical neurons against OGD/R injury, possibly by decreasing apoptosis and oxidative stress, while activating Akt signaling and mitochondrial pathways. Our results suggest that Au-NPs may be potential therapeutic agents for ischemic stroke.

Keywords Gold nanoparticles · Ischemic stroke · Primary rat cortical neurons · Neuronal apoptosis · Oxidative stress · Mitochondria

Introduction

Stroke is the second leading cause of death worldwide, following ischemic heart disease [1], and is primarily caused by thrombosis or embolism [2]. According to the World Health Organization, approximately 15 million people experience stroke each year [3]. Additilly, stroke is the third most common cause of disability, following ischemic heart disease and lower respiratory infections, thereby placing a heavy economic burden on the patient's family and community [4, 5]. Blood flow provides brain cells with oxygen, which is essential for energy production. Therefore, a combination of blood flow restoration and reoxygenation is the globally approved strategy for the treatment of acute ischemic stroke [6–8]. Paradoxically, the subsequent reperfusion can result in additional brain injury, including hemorrhagic transformation, blood–brain barrier (BBB) disruption, and massive brain edema, in what is known as cerebral ischemic-reperfusion (I/R) injury [9–12]. Efforts to treat I/R injury are currently underway. Treatment of ischemic stroke is difficult in part because I/R-induced cerebral injury is related to diverse pathological processes, including cellular apoptosis,

✉ Zhengxia Liu
zhengxl1@njmu.edu.cn

✉ Xiang Lu
luxiang66@njmu.edu.cn

1 Department of Geriatrics, The Second Affiliated Hospital, Nanjing Medical University, Nanjing 210003, Jiangsu, People's Republic of China

2 Department of Neurology, The Second Affiliated Hospital, Nanjing Medical University, Nanjing 210003, Jiangsu, People's Republic of China

3 Key Laboratory for Aging & Disease, Nanjing Medical University, Nanjing 210003, Jiangsu, People's Republic of China

4 Department of Medicine, Physiology and Biophysics, UC Irvine Diabetes Center, Center for Epigenetics and Metabolism, University of California Irvine, Irvine, CA 92697, USA

5 Department of Geriatrics, The Second Affiliated Hospital, Nanjing Medical University, 121 Jiang Jia Yuan, Nanjing 210011, Jiangsu, China

inflammation, oxidative stress, excitotoxicity, calcium overload, and mitochondrial dysfunction [13–17]. Thus, novel therapeutic agents that can effectively treat cerebral I/R-induced injury are in high demand. Although numerous studies have been performed in recent years, few effective treatments are available [18].

Gold nanoparticles (Au-NPs) have been actively investigated in a wide variety of biomedical applications owing to their unique physicochemical characteristics, good biocompatibility, and the simplicity of their synthesis [19–21]. Today, many disciplines contribute to Au-NP research, including the fields of bio-sensing, photo-imaging, in vitro diagnostics, targeted drug delivery, and even intrinsic treatment [22–27]. Au-NPs have received a great deal of attention as anti-inflammatory agents [28] due to their ability to inhibit the expression of inflammation-related proteins, such as nuclear factor-κB, and the subsequent inflammatory reactions [29]. Fernandez et al. [30] found that 12-nm Au-NPs could induce an increase in IL-4 accompanied by a lack of IL-12p70 and IFN-γ expression in dendritic cells (DCs). However, the same report showed that exposure to 2-nm Au-NPs resulted in an opposite effect on cytokine levels in DCs. These observations suggest that Au-NPs of different sizes may have different effects on the inflammatory response. Moreover, several studies have demonstrated that Au-NPs have potential antioxidant effects, as they are effective in restraining reactive oxygen species (ROS) [31]. Gao et al. [32] reported that 22-nm Au-NPs reduced Aβ-mediated peroxidase activity in vitro, while Rizwan et al. [33] demonstrated that treatment with Au-NPs inhibited high glucose-induced ROS/RNS production, antioxidant depletion, biomolecular damage, inflammation, and apoptosis in macrophages. Ferreira et al. [34] investigated the effects of acute and long-term administration of Au-NPs in adult rats, and found, in particular, that acute administration of 10-nm Au-NPs and 30-nm Au-NPs increased superoxide dismutase (SOD) activity. Long-term administration of 30-nm Au-NPs also increased SOD activity. Furthermore, Au-NPs were shown to prevent cognitive deficits, oxidative stress, and inflammation in a rat model of sporadic Alzheimer's disease [35]. Given the anti-inflammatory and antioxidant effects demonstrated in these studies, Au-NPs may have therapeutic potential for the treatment of cerebral I/R injury.

Our previous work demonstrated that 20-nm Au-NPs significantly alleviated cerebral I/R injury in a rat model of middle cerebral artery occlusion (MCAO) [27]. In contrast, 5-nm Au-NPs resulted in aggravated neurological deficits and enlarged infarction volumes compared with an untreated I/R group. Although these results indicate that apoptosis, inflammation, and oxidative stress may be involved in these processes, the mechanisms underlying the role of Au-NPs in ischemic stroke remain poorly understood. Under pathological conditions, increased oxidative stress can lead to mitochondrial dysfunction. Mitochondria can then generate excessive ROS, leading to a vicious cycle. The term 'ROS-induced ROS release' reflects such endless cycle of ROS production [36]. Oxidative stress injury to the mitochondria and the subsequent mitochondrial dysfunction are involved in ischemic stroke. The objectives of the present study were to investigate the potential effects and the corresponding mechanisms of Au-NPs on primary rat cortical neurons exposed to oxygen–glucose deprivation/reperfusion (OGD/R) which is an in vitro technique commonly used to mimic ischemic injury.

Materials and Methods

Ethical Disclosure

All experiments were conducted in accordance with the guidelines approved by Nanjing Medical University Animal Care and Use Committee.

Preparation of Au-NPs

We synthesized 5-nm Au-NPs using the $NaBH_4$ reduction method [37]. Under constant stirring at room temperature (RT), 2 mL of 100 mM fresh $HAuCl_4$ solution was quickly added to an 80 mL solution containing 0.25 mM $HAuCl_4$ and 0.25 mM trisodium citrate. The resulting Au-NPs were aged at RT for at least 2 h for subsequent experiments.

20-nm Au-NPs were synthesized using the classic citrate reduction method [38]. For the synthesis, 100 mL of 0.25 mM $HAuCl_4$ aqueous solution was heated to boiling. Next, 4.5 mL of 1% (weight/volume) citrate solution was added to the prepared solution, and boiling was continued until the color of the solution changed to ruby red. The citrate-capped Au-NP solution was then naturally cooled to RT for future use.

Characterization and Dispersion of the Au-NP Suspension

The morphology of the Au-NPs was observed using a previously reported method [39]. Briefly, we used transmission electron microscopy (TEM; JEM-2100EX, JEOL, Tokyo, Japan) to analyze the size and shape of the Au-NPs at an accelerating voltage of 200 kV. Ultraviolet–visible (UV–Vis) spectra were acquired with a Shimadzu UV-3600 spectrophotometer in the 300–1100 nm range. The Au-NP stock solution was stirred with 5% (w/v) bovine serum albumin for 30 min, then centrifuged at 20,000×*g* for 40 min to obtain the 5-nm Au-NPs and 9000 g for 20 min to obtain 20-nm Au-NPs. After removing the supernatant, the Au-NP precipitate was then resuspended in a different volume of

neurobasal-A medium supplemented with 2% B27 by agitation with a vortex mixer. Finally, the concentration of the Au-NP suspension was identified via inductively coupled plasma mass spectrometry (ICP-MS). The Au-NP suspensions were freshly prepared for each cell culture.

Primary Rat Cortical Neuron Cultures

Briefly, rat cortical tissues were obtained from neonatal Sprague-Dawley rats and maintained in phosphate-buffered saline (PBS) on ice, then sectioned and incubated for 10 min in 0.25% (w/v) trypsin in a 37 °C water bath, followed by the addition of Dulbecco's Modified Eagle Medium: Nutrient Mixture F-12 (DMEM/F12) (1:1) containing 10% (v/v) fetal bovine serum (FBS) and centrifugation at 200×*g* for 5 min at 4 °C. After removing the supernatant, the cells were resuspended in DMEM/F12 with 10% FBS, 100 U/mL penicillin, and 100 U/mL streptomycin. The cells were then seeded on poly-D-lysine-coated plates at a density of 5×10^4 cells/well in a 96-well plate and 1×10^6 cells/well in a 6-well plate. Cell cultures were maintained at 37 °C in a 5% CO_2/95% air humidified incubator chamber (Thermo Scientific 3110, MA, USA). After 4 h, the culture medium was changed to serum-free neurobasal-A medium supplemented with 2% B27 (Gibco, Life Technologies, Paisley, UK). The following experiments were performed with neurons that had been in primary culture for 72 h.

Immunofluorescence Staining

Neuron-specific enolase (NSE) translocation was observed by immunofluorescence staining. Rat cortical neurons grown on coverslips were fixed in 4% paraformaldehyde for 30 min at RT and blocked with 5% BSA and 1% Triton X-100 for 1 h at RT. Next, cells were incubated with anti-NSE rabbit polyclonal antibody (1:100 diluted) overnight at 4 °C and then with Dylight 549-labeled goat anti-rabbit secondary antibody (1:100) for 1 h at RT in the dark. DAPI was added for nuclear staining. The neurons were observed under a fluorescence microscope (Leica DM2500). For quantitative analysis, the purity of neurons was calculated from three random fields.

Oxygen–Glucose Deprivation and Reperfusion (OGD/R) Cell Models Mimicking Ischemia-Reperfusion Injury

The in vitro ischemia model was obtained as described previously [40]. The growth culture medium of the cells was replaced with glucose-free serum-free medium (Gibco), and the plates were placed in an oxygen-free chamber next to a sachet containing ascorbic acid (Mitsubishi gas chemical company, Tokyo, Japan). An oxygen indicator (Mitsubishi gas chemical company) was also placed in the chamber. The lid of the chamber was then closed tightly, and the chamber was returned to the 5% CO_2/95% air incubator at 37 °C. The completely anaerobic condition in the chamber was verified by the color of the indicator changing from lilac to pink. Meanwhile, the onset time for oxygen–glucose deprivation (OGD) was recorded. After 4 h of deprivation, the medium was replaced with normal growth culture medium with or without Au-NPs, under normoxic conditions, for 48 h. For the following in vitro experiments, the cortical neuron cultures were categorized as follows: control, OGD/R, OGD/R+5-nm Au-NP, and OGD/R+20-nm Au-NP.

Uptake and Quantitative Analysis of Au-NPs

The uptake of Au-NPs by rat cerebral cortical neurons was verified using TEM. After exposure to Au-NPs for 48 h, the cells were collected enzymatically and fixed in 3.7% (v/v) paraformaldehyde in PBS for 20 min at RT. The cells were then prepared for TEM analysis as described previously [41]. Cells were fixed in 1% (w/v) osmium tetroxide for 2 h, dehydrated in a graded series of 30, 50, 70, 80, and 90% ethanol, and treated three times with 100% ethanol for 15 min each. The samples were then embedded in a mixture of resin in propylene oxide polymerized at 80 °C. Ultrathin sections for TEM were prepared using a diamond knife, and the samples were analyzed using TEM (JEM-2100EX, JEOL, Tokyo, Japan) with an accelerating voltage of 80 kV. The internalization of Au-NPs was quantified using ICP-MS.

Cell Viability Assay

Cell viability was assessed using the Cell Counting Kit-8 (CCK8, Vazyme) according to the manufacturer's instructions, as described previously [41]. Primary cortical neurons were isolated as described above, then seeded on a 96-well plate at a density of 5×10^4 cells per well in a 100 µL volume. After being subjected to OGD for 4 h, cells were incubated in neurobasal-A medium containing 2% B27 with or without various concentrations of 5 nm or 20 nm Au-NPs. After a 48-h incubation, 10 µL of 2-(2-methoxy-4-nitrophenyl)-3-(4-nitrophenyl)-5-(2,4-disulfophenyl)-2H-tetrazolium, monosodium salt (WST-8) was added to each well before an additional 1-h incubation at 37 °C in the 5% CO_2/95% air, humidified incubator chamber. Optical density (OD) was measured with a microplate reader (Bio-Rad, CA, USA) at 450 nm. The mean absorbance value for each concentration of Au-NPs was divided by the mean value of the control cells, and is thus presented as a percentage, where the control group corresponds to 100%. The data were then plotted using Prism 5.0 (GraphPad Software, San Diego, CA, USA).

Cell Apoptosis Assay

Flow cytometry analysis was used to assess apoptotic rates using the Annexin V-fluorescein isothiocyanate (FITC)/propidium iodide (PI) double staining apoptosis detection kit (BD Biosciences Pharmingen, San Jose, CA, USA), according to the manufacturer's instructions. In brief, the cells from each of the four groups were treated with or without Au-NPs for 48 h after the 4-h OGD period. Subsequently, cells were collected following trypsinization (0.25% trypsin), then centrifuged at 200×*g* for 5 min at 4 °C and washed twice with pre-cold PBS. After removing the supernatant, cells were resuspended in the binding buffer at a concentration of 1×10^6 cells/mL, and then stained with 5 μL of Annexin V-FITC for 15 min in the dark at RT, followed by the addition of 5 μL of PI and 200 μL of binding buffer. Finally, the stained apoptotic cells were identified by the FACSCanto II system (BD Bioscience, USA), and data were analyzed using the FlowJo software.

Assessment of the Mitochondrial Membrane Potential

The mitochondrial membrane potential (MMP, ΔΨm) was determined using a JC-1 detection kit (Beyotime, Jiangsu, China) according to the manufacturer's instructions, as described previously [42]. Briefly, cells were harvested and washed twice with PBS, then 1 μL of JC-1 was added to 500 μL of incubation buffer, and the cells were incubated for 20 min in the mixture at 37 °C in the dark. After centrifugation, the cells were resuspended in the incubation buffer and immediately analyzed using the FACSCanto II system (BD Bioscience, USA). Data were analyzed using the FlowJo software.

Measurement of Reactive Oxygen Species Generation

The levels of intracellular ROS were measured using an ROS assay kit (Beyotime) following the manufacturer's protocol with minor modifications. After removing the supernatant from the 6-well culture plate, the neurons were washed with Hanks' Balanced Salt Solution (HBSS) and then incubated with dichloro-dihydro-fluorescein diacetate at a final concentration of 10 μM for 30 min at 37 °C in the 5% CO_2/95% air incubator chamber. Subsequently, the neurons were washed twice with HBSS to remove excess dichloro-dihydro-fluorescein diacetate and harvested for final analysis using the FACSCanto II system (BD Bioscience, USA). The results were reported as mean fluorescence intensity (MFI) and analyzed using the FlowJo software.

Measurement of Malondialdehyde Generation

Lipid peroxidation was evaluated by measuring malondialdehyde (MDA) levels using the thiobarbituric acid-reactive substance method (Beyotime) [43]. MDA reacts with thiobarbituric acid to form a colorimetric (532 nm) product. The cells, divided into four experimental groups as described above, were collected and lysed with RIPA lysis and extraction buffer on ice followed by centrifugation at 12,000×*g* for 5 min. Next, the supernatant was mixed with reagents C and D, incubated at 100 °C for 50 min, and rapidly cooled in ice water. Subsequently, the mixture was centrifuged at 500×*g* for 15 min at 4 °C. The absorbance of the supernatant was measured at 532 nm, and the concentration of MDA was calculated according to a standard curve. The results are expressed as nmol/mg of protein.

Measurement of Superoxide Dismutase Generation

SOD activity was measured with the xanthine oxidase method using an SOD assay kit (Beyotime). Cells were collected and homogenized in ice-cold PBS, and then centrifuged at 10,000×*g* for 5 min at 4 °C. The upper aqueous layers, containing SOD enzymes, were collected for enzymatic assays. Assays were conducted according to the manufacturer's protocol, and the total protein concentration was determined using the Bradford method. The absorbance was then measured at 450 nm using a microplate reader. SOD activity is expressed as enzyme units/mg of cell protein.

Measurement of Caspase-3 Generation

Caspase-3 activity was determined using a caspase-3 colorimetric assay kit (Beyotime), according to the manufacturer's instructions. Briefly, cells were lysed, and the substrate was cleaved by caspases before being centrifuged at 2000×*g* for 5 min at 4 °C. Fifty μL of supernatant, 50 μL of reaction buffer, and 5 μL of caspase-3 substrate were mixed and incubated for 1 h in the dark at 37 °C. Afterwards, absorbance was measured at 405 nm by a microplate reader. Caspase-3 activity is expressed as a percentage of the control group result.

Aconitase Activity Assay

An aconitase activity assay kit (BioVision, Milpitas, CA, USA) was used to measure mitochondrial aconitase activity, as described previously [44]. Cells were collected after treatment and centrifuged at 1000×*g* for 10 min at 4 °C. After removing the supernatant, cells were resuspended in 100 μL of assay buffer on ice. Next, cells were homogenized before centrifugation at 800×*g* for 10 min at 4 °C. The resulting supernatant was used to measure aconitase

activity at 450 nm using a microplate reader. The OD values were normalized to the protein concentration of each sample, and the results are expressed as a percentage of the control group result.

Quantitative Real-Time PCR Assay

Forty-eight hours after the 4 h-OGD period, total RNA from primary cortical neurons was extracted using Trizol. The purity of the extracted RNA was determined, and then reverse transcription polymerase chain reaction (RT-PCR) was performed using a Hiscript Q RT Super Mix for qPCR (Vazyme, China) following the manufacturer's instructions. mRNA expression levels were quantified by real-time PCR with the FastStart Universal SYBR Green Master (ROX) (Roche, Germany) and the ABI 7500 real-time PCR system (Applied Biosystems, USA). A no-template control was analyzed in parallel for each gene, and the GAPDH gene was selected as the housekeeping gene. Eventually, the unknown template was calculated through the standard curve for quantitative analysis.

The primer sequences are shown the following: AIF Fwd, ATGTCCGTCGCACTCAGCAA, AIF Rv, TCAAGGCAG GCTGGCAAT; Bax Fwd, GGCCCACCAGCTCTGAAC AGAT, Bax Rv, TCAGCCCATCTTCTTCCAGAT; Bcl-2 Fwd, ATGGCGCAAGCCGGGAGAACAGGGTATGAT AA, Bcl-2 Rv, TCACTTGTGGCCCAGGTATG; Caspase-3 Fwd, ATGGACAACAACGAAACCTCC, Casepase-3 Rv, TTAGTGATAAAAGTACAGTTCTTTTGTGAGC; Cytochrome c Fwd, GCAGTGTCCTTGTCCTCGAAGT, Cytochrome c Rv, CTTGAGTCCCATGCGTTTT; GAPDH Fwd, GAAAGACAACCAGGCCATCAG, GAPDH Rv, TCA TGAATGCATCCTTTTTTGC.

Western Blot Analysis

Forty-eight hours after the 4 h-OGD period, protein samples from rat primary cortical neurons were extracted and homogenized in lysis buffer. Western blot analyses were performed using 50 μg of the extracted protein samples. The supernatants were then separated by 10% SDS–PAGE and transferred to an Immobilon-FL membrane. After blocking with Tris-buffered saline (TBS) containing 5% non-fat milk, the membranes were probed overnight at 4 °C with primary antibodies: BAX (1:2000, Abcam), p-Akt (1:2000, Cell Signaling), Akt (1:1000, Cell Signaling), p-GSK3β (1:1000, Cell Signaling), GSK3β (1:1000, Cell Signaling), GAPDH (1:5000, CMCTAG). The membrane was then incubated at room temperature for 1 h with horseradish peroxidase-conjugated antibodies. Protein expression was assessed using an enhanced chemiluminescence method with the ECL kit (BioRad, USA) and imaged using the ChemiDoc XRS imager (Bio-Rad, USA).

Measurement of Mitochondrial Oxygen Consumption by a Seahorse XF96 Analyzer

Mitochondrial oxygen consumption was measured using a Seahorse XF96 Extracellular Flux analyzer (Seahorse Bioscience, North Billerica, MA, USA) as described previously [45, 46]. After dividing the cells into four groups as described above, neurons were cultured for 48 h. Subsequently, the 96-well plate was loaded into the Seahorse XF96 analyzer and various factors were assessed every 8 min, including basal respiration, mitochondrial respiration, ATP generation, proton leakage, maximal respiration, and reserve capacity. Agents were added every three assessments in the following sequence: oligomycin (2 μM), FCCP (2 μM), antimycin A (0.5 μM), and rotenone (0.5 μM).

Statistical Analysis

Each experimental condition was replicated at least three times from three independent culture preparations. Data are expressed as mean ± standard error (SEM). All treatment groups were compared with the control group using one-way ANOVA with Dunnett's post-test. P-values < 0.05 were considered statistically significant. All statistical analyses were performed using Prism 5.0 (GraphPad Software).

Results

Synthesis and Characterization of Au-NP Suspensions

TEM was performed to confirm the primary particle size and to observe the general morphology of the particles. All samples exhibited spherical shape and narrow size distributions (Fig. 1a, b). The successful generation of 5- and 20-nm Au-NPs was also qualitatively examined using UV–Vis spectroscopy (Fig. 1c, d). The Au-NPs were well dispersed in the neurobasal medium. The concentrations of 5- and 20-nm Au-NP suspensions were 200, 400, 800, 1600, and 2400 μg/L, as quantified by ICP-MS.

Assessment of the Purity of Rat Cortical Neurons

To observe the morphology and evaluate the purity of neurons, cells were isolated and cultured in serum-free culture media. As shown in Fig. 2a, neurons grew well on the fifth day. Cells were then incubated with anti-NSE rabbit polyclonal antibody. For quantitative analysis, the purity of

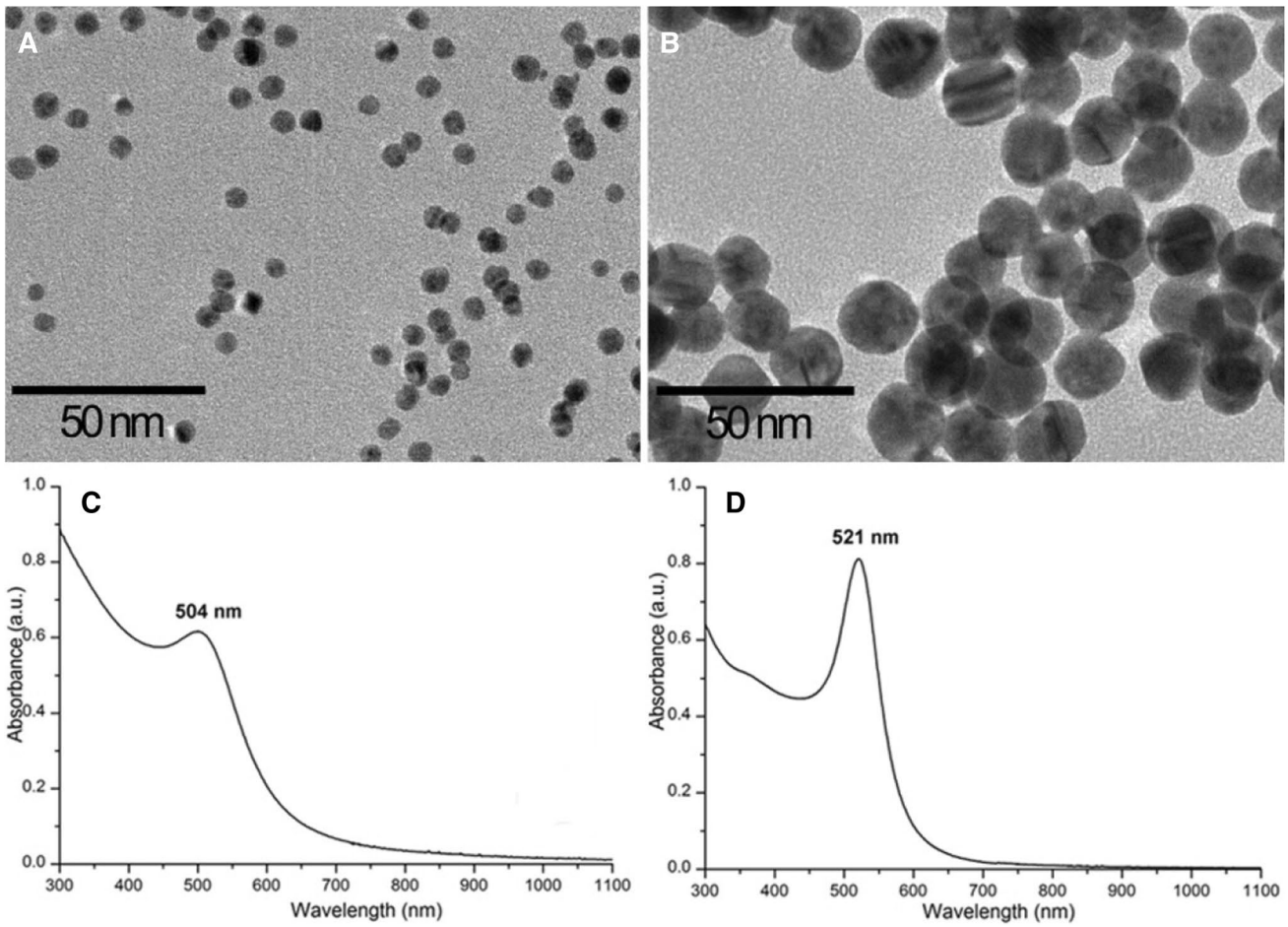

Fig. 1 Characterization of gold nanoparticles (Au-NPs) by transmission electron microscope (TEM) and UV–Vis analysis. **a** TEM images of 5-nm Au-NPs. The scale bar represents 50 nm. **b** TEM images of 20-nm Au-NPs. The scale bar represents 50 nm. **c** UV–Vis absorption spectrum of 5-nm Au-NP solution and its digital picture (inset). **d** UV–Vis absorption spectrum of 20-nm AuNP solution and its digital picture (inset)

neurons was calculated from three random fields, and was as high as 82.7 ± 2.3% (Fig. 2b).

Internalization of Au-NPs

Au-NPs have received a great deal of attention for biomedical applications due to their good biocompatibility [47]. Cell internalization of the Au-NPs in rat cortical neurons was investigated using TEM imaging. The results showed that the uptake and intracellular distribution of the Au-NPs in the neurons exhibited pharmacodynamic action (Fig. 3). Au-NPs primarily enter cells by phagocytosis. In the neurons, they were stably localized in the cytosol, membranous vesicles, and lysosomes in the form of aggregates or single particles, but were not observed in the nucleus, an observation that contributes to our understanding of the interaction of Au-NPs with neurons. Intriguingly, the 20-nm Au-NPs, but not the 5-nm AuNPs, were observed in the mitochondria (Fig. 2f): This is likely explained by the timing and angle not being appropriate.

Cell Viability

To detect the effects of Au-NPs on normal neurons, cells were treated with a range of concentrations of 5- or 20-nm Au-NPs (200, 400, 800, 1600, and 2400 μg/L) for 48 h. As shown in Fig. 4a, cell viability increased after 20-nm Au-NP treatment and decreased after 5-nm Au-NP treatment. Cell viability was significantly reduced after OGD/R treatment ($P < 0.05$, Fig. 4b), and divergent trends were observed for the differently-sized Au-NPs. Cell survival was notably facilitated by 20-nm Au-NP treatment at concentrations of 800, 1600, and 2400 μg/L ($P < 0.001$). These results indicate that 20-nm Au-NPs exert a protective effect on rat cerebral cortical neurons. In contrast, 5-nm Au-NPs induced a dose-dependent decrease of neuron viability. The threshold concentration of 5-nm Au-NPs inducing significant toxicity

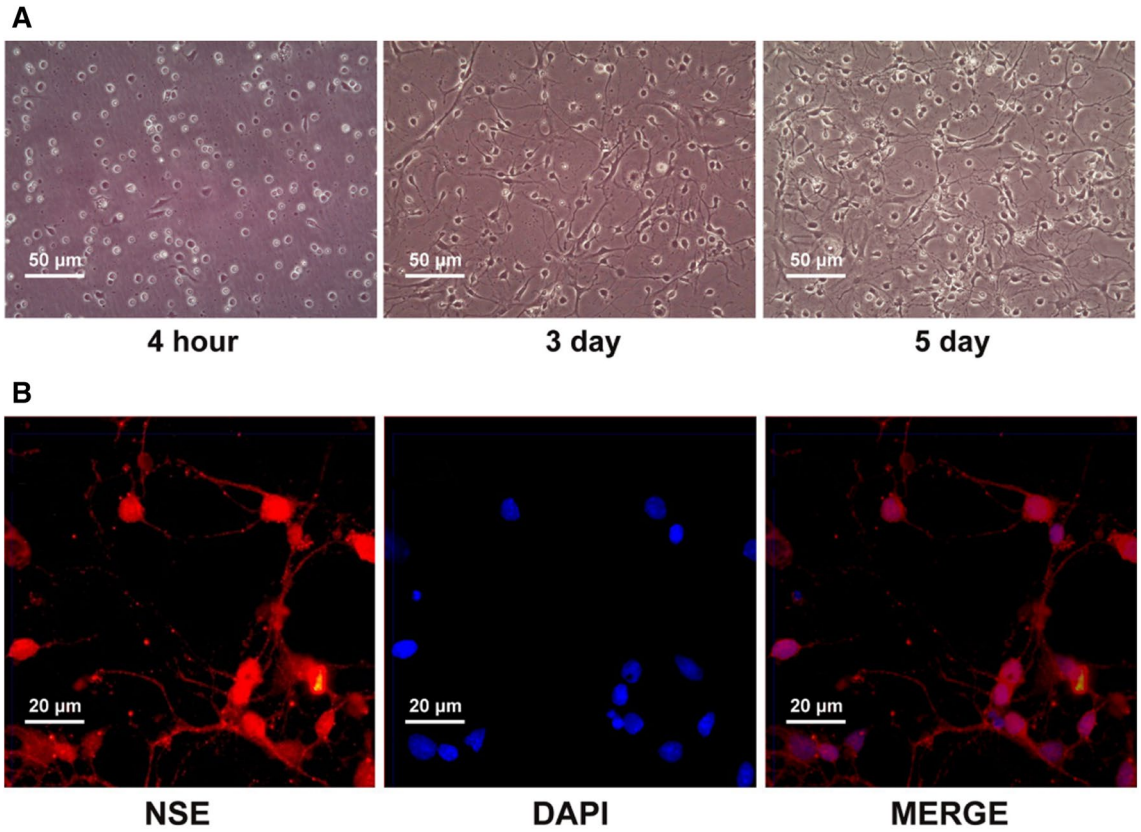

Fig. 2 Identification of the purity of rat cortical neurons. **a** Primary rat cortical neurons were seeded in a 6-well plate at a density of 1 × 106 cells/well. The images were taken 4 h, 3 days, and 5 days after seeding. The scale bar represents 50 μm. **b** Neuron-specific enolase location was observed by immunofluorescence staining. The scale bar represents 20 μm

after OGD/R was 800 μg/L ($P < 0.05$), and further concentration increases significantly decreased cell viability. In the 2400 μg/L group, cell viability was approximately 40% of that in the control group ($P < 0.001$). Considering the above results, we selected 800 μg/L for the 20-nm Au-NPs and 2400 μg/L for the 5-nm Au-NPs for further OGD/R experiments, which were performed to obtain a deeper understanding of the mechanisms leading to the effects of Au-NPs on cerebral I/R injury.

Cerebral Inflammation After OGD/R Injury

As shown in Fig. 5a, compared with the OGD/R group, the mRNA levels of the pro-inflammatory factors IL-1β and TNF-α were significantly increased in the 5-nm Au-NP group ($P < 0.01$ for both factors) and decreased in the 20-nm Au-NP group ($P < 0.05$ for both factors). In addition, the levels of the anti-inflammatory cytokines IL-4 and IL-10 were markedly decreased in the 5-nm Au-NP group ($P < 0.05$ and $P < 0.01$, respectively) and increased in the 20-nm Au-NP group ($P < 0.05$ and $P < 0.01$, respectively) after OGD/R injury (Fig. 5b). These results clearly indicate that 20-nm Au-NP treatment relieved neuroinflammation after OGD/R injury by modulating the immune inflammatory response.

Apoptosis of Neurons

We further evaluated whether Au-NPs could affect cortical neurons by influencing neuronal apoptosis. We observed that the number of necrotic cells decreased significantly in the 20-nm Au-NP group ($P < 0.05$), whereas apoptosis was increased in the 5-nm Au-NP group ($P < 0.01$, Fig. 6a, c). Furthermore, the JC-1 assay of mitochondrial membrane potential indicated that 20-nm Au-NPs led to an increase in JC-1 aggregates ($P < 0.05$) and a decrease in JC-1 monomers ($P < 0.05$), while the 5-nm Au-NPs exerted opposite effects (Fig. 6b, d, e).

As shown in Fig. 7a, b, d, and e, the mRNA levels of the pro-apoptotic genes *Aif*, *Bax*, caspase-3 and cytochrome c were dramatically downregulated in the 20-nm Au-NP group compared with the OGD/R group ($P < 0.01$, $P < 0.05$, $P < 0.05$, and $P < 0.05$, respectively), and the anti-apoptotic factor *Bcl2* mRNA was upregulated ($P < 0.01$, Fig. 7c), whereas the opposite changes were observed in the 5-nm Au-NP group compared with the OGD/R group

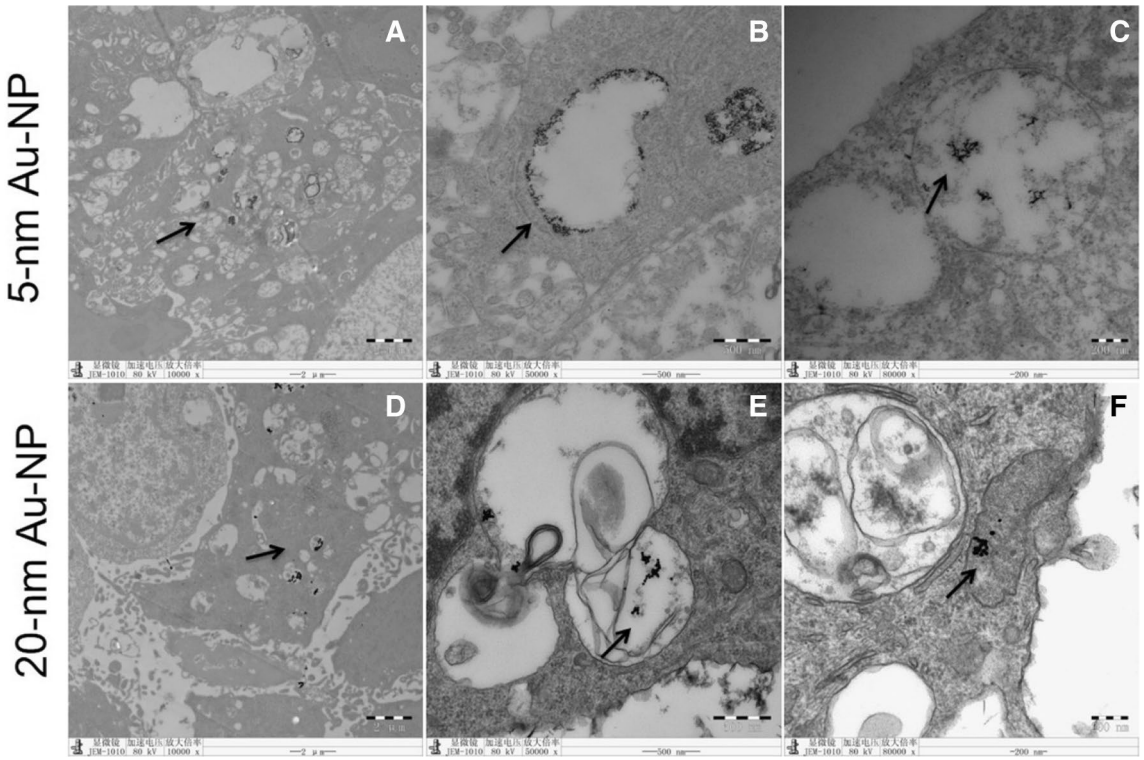

Fig. 3 Transmission electron microscopy images of internalized Au-NPs in primary rat cortical neurons. **a–c** 5-nm Au-NPs in rat cortical neurons. The scale bars represent 2 μm, 500 nm, and 200 nm, respectively. **d–f** 20-nm Au-NPs in rat cortical neurons. The scale bars represent 2 μm, 500 nm, and 200 nm, respectively. Black arrows point to the location of the internalized Au-NPs

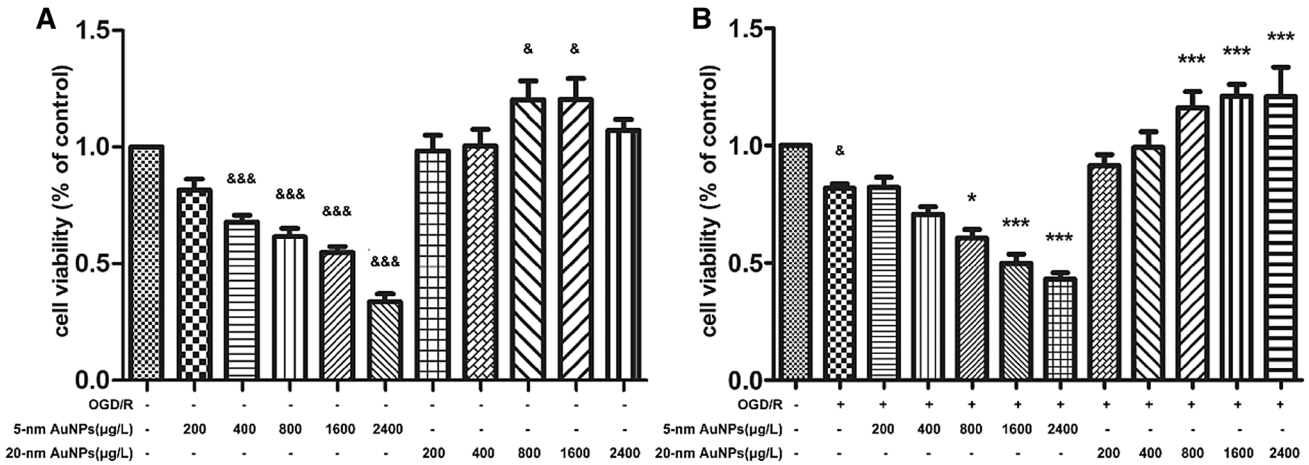

Fig. 4 Effects of different concentrations of Au-NPs on cell viability in primary rat cortical neurons exposed to oxygen-glucose deprivation/reperfusion (OGD/R). **a** Neurons that were not exposed to OGD/R. The results are expressed as the mean ± standard error of the mean from at least triplicate independent experiments. $^{\&}P < 0.05$ versus control group, $^{\&\&\&}P < 0.001$ versus control group. **b** Neurons that were exposed to OGD/R. The results are expressed as the mean ± standard error of the mean from at least triplicate independent experiments. $^{*}P < 0.05$ versus OGD/R group, $^{***}P < 0.001$ versus OGD/R group, $^{\&}P < 0.05$ versus the control group

(Fig. 7a–e). In addition, *Bcl2* mRNA levels increased in the OGD/R group compared with the control group, possibly due to the protective stress response ($P < 0.001$, Fig. 7c). The observed changes in the protein levels of cleaved caspase-3 and BAX were similar to those observed in mRNA levels (Fig. 7f–h).

In order to explore the underlying mechanisms, we evaluated whether Au-NPs could regulate the Akt signaling

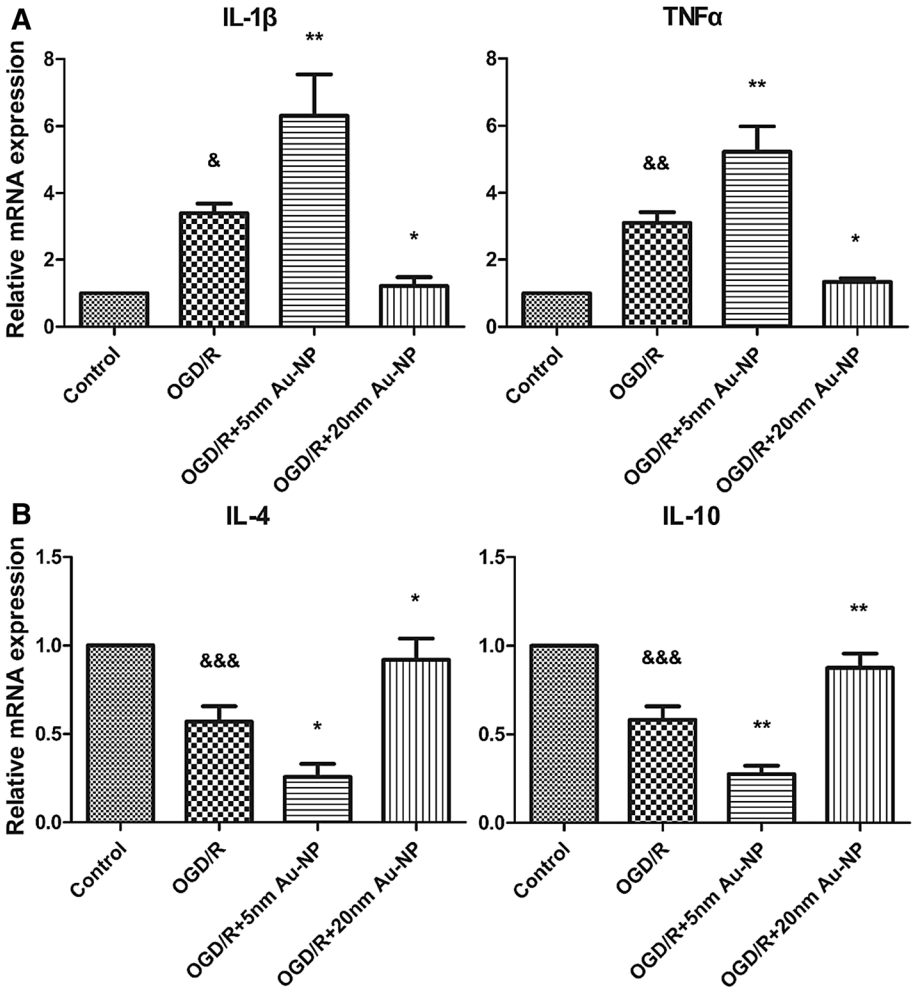

Fig. 5 Effects of Au-NPs on the gene levels of the inflammatory mediators **a** (IL-1β, TNF-α), **b** (IL-4 and IL-10) in primary rat cortical neurons after OGD/R injury. The results are expressed as mean ± standard error of the mean from at least triplicate independent experiments. $^{\&}P < 0.05$ versus control group, $^{\&\&}P < 0.01$ versus control group, $^{\&\&\&}P < 0.001$ versus control group, $^{*}P < 0.05$ versus the OGD/R group, $^{**}P < 0.01$ versus the OGD/R group

pathway. Western blotting showed that phosphorylated Akt and its downstream signaling molecule GSK3β were upregulated in the 20-nm Au-NP group compared with the OGD/R group ($P < 0.01$, $P < 0.05$, respectively, Fig. 7g, i, j), while the opposite trend was observed in primary neurons treated with 5-nm Au-NPs ($P < 0.001$ for both proteins). These data suggest that 20-nm Au-NPs could alleviate the apoptosis of rat cerebral cortical neurons after OGD/R through the activation of Akt signaling.

Cellular Oxidative Stress Level

In order to investigate the antioxidant activity of Au-NPs in rat cerebral cortical neurons, we tested the levels of MDA, SOD, aconitase, and ROS. As shown in Fig. 8a, the 5- and 20-nm Au-NPs led to increased ($P < 0.01$) and decreased ($P < 0.05$) production of MDA, respectively, in rat cerebral cortical neurons compared with those in the OGD/R group. Similar changes were observed in ROS production (Fig. 8d, e). In addition, SOD levels were lower in the 5-nm Au-NP group ($P < 0.01$) and higher in the 20-nm Au-NP group ($P < 0.01$) than in the OGD/R group (Fig. 8b). The same trends were observed for aconitase activity (Fig. 8c). Taken together, these results suggest that 20-nm Au-NPs ameliorate oxidative stress in neurons after OGD/R injury.

Au-NPs Alter Mitochondrial Respiration Function in Neurons

To measure the mitochondrial respiration function in neuron cells, we used a Seahorse XF96 Extracellular Flux analyzer. As illustrated in Fig. 7, 20-nm Au-NPs induced a significant increase in the basal respiration of the neurons ($P < 0.001$). Basal respiration is strongly controlled by ATP turnover and partly by substrate oxidation and proton leakage; therefore, basal oxygen consumption rates (OCR) are sensitive to ATP demand but rather insensitive to small changes in the mitochondrial respiratory chain or proton leakiness [48]. In order to assess the effect of Au-NPs on these specific parameters, OCR was recorded after the addition of several mitochondrial inhibitors (Fig. 9a). Notably, we found that 20-nm Au-NPs could significantly improve mitochondrial respiration ($P < 0.001$),

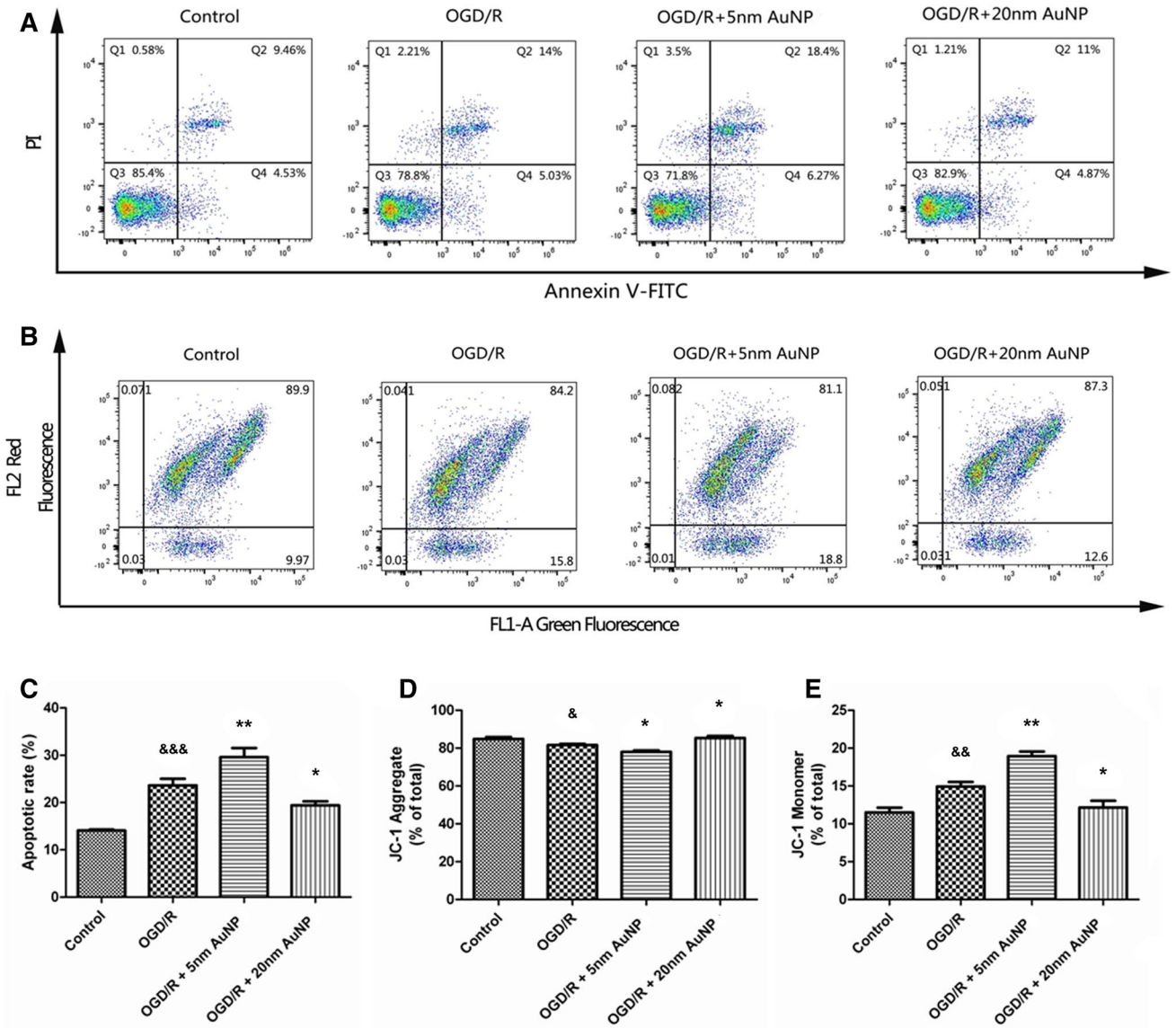

Fig. 6 The flow cytometry detection for Au-NPs on neurons exposed to OGD/R injury. **a**, **c** Cell injury was evaluated in terms of apoptotic rate using Annexin V-FITC double staining. **b**, **d**, **e** Cell injury was evaluated in terms of mitochondrial membrane potential by detecting JC-1. The results are expressed as mean ± standard error of the mean from at least triplicate independent experiments. $^{\&}P < 0.05$ versus control group, $^{\&\&}P < 0.01$ versus control group, $^{\&\&\&}P < 0.001$ versus control group, $^{*}P < 0.05$ versus the OGD/R group, $^{**}P < 0.01$ versus the OGD/R group

ATP generation ($P < 0.05$), proton leakage ($P < 0.01$), and maximal respiration ($P < 0.001$). In addition, proton leakage and reserve capacity were increased in the 5-nm Au-NP group, possibly due to the stress response. These results indicate that 20-nm Au-NPs exert strong protection on the mitochondrial respiration function against OGD/R-induced injury in rat cerebral cortical neurons.

Discussion

Our previous study demonstrated that 20-nm Au-NPs markedly alleviated cerebral I/R injury in a rat MCAO model. However, 5-nm Au-NPs were found to aggravate the neurological deficits, resulting in enlarged infarction

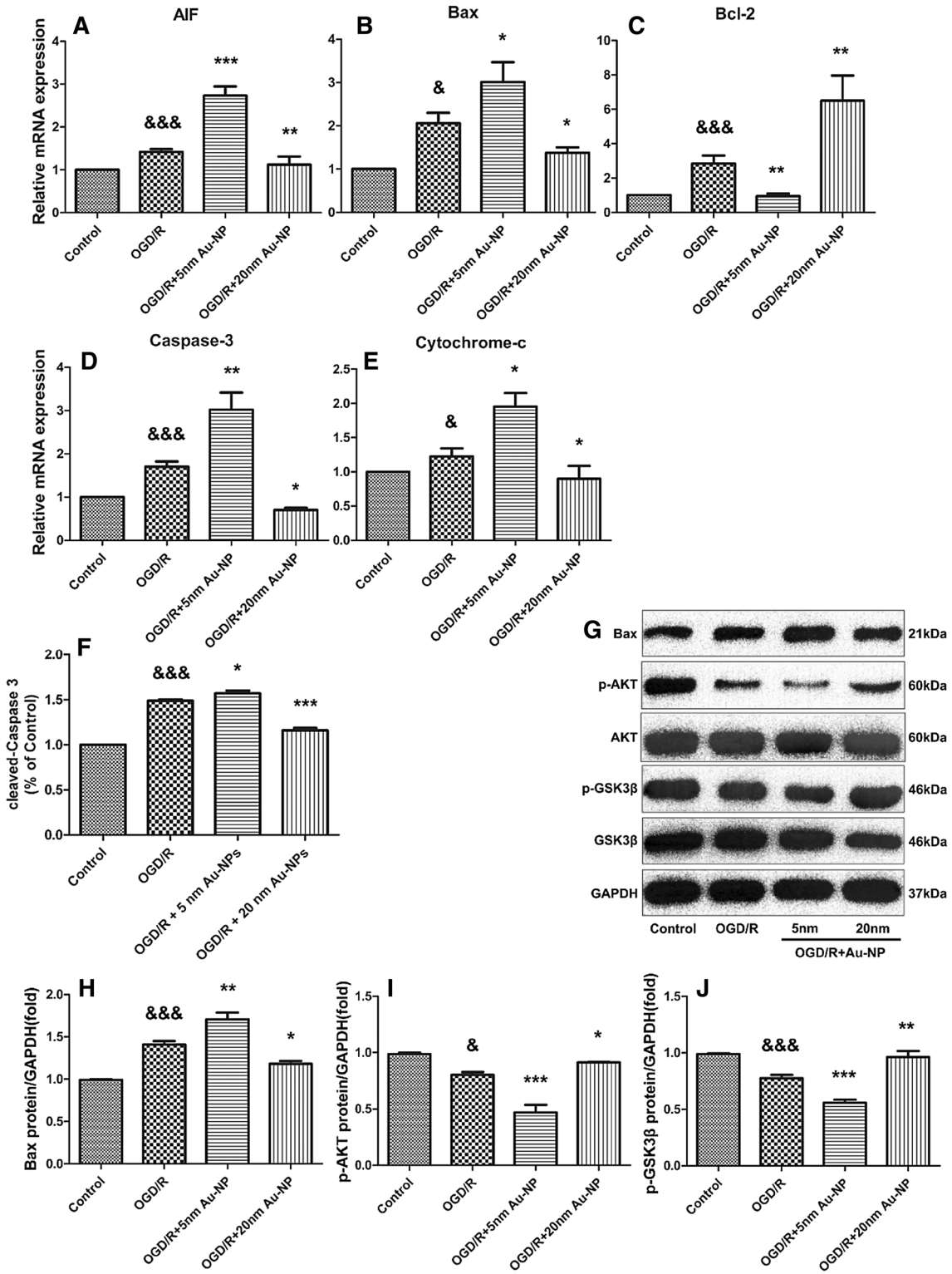

Fig. 7 Effects of Au-NPs on neuronal apoptosis. **a**–**e** Effects of Au-NPs on the gene levels of apoptosis-related genes AIF, Bax, Bcl-2, caspase-3 and cytochrome *c* in primary rat cortical neurons after OGD/R injury. **f** Cell injury was evaluated in terms of caspase-3 activity. **g** Western blots, showing the expression of Bax, p-AKT and p-GSK3β in primary rat cortical neurons after OGD/R injury. **h**–**j** Quantitative analysis of the western blots. $^{\&}P < 0.05$ versus control group, $^{\&\&\&}P < 0.001$ versus control group, $^{*}P < 0.05$ versus the OGD/R group, $^{**}P < 0.01$ versus the OGD/R group, $^{***}P < 0.01$ versus the OGD/R group

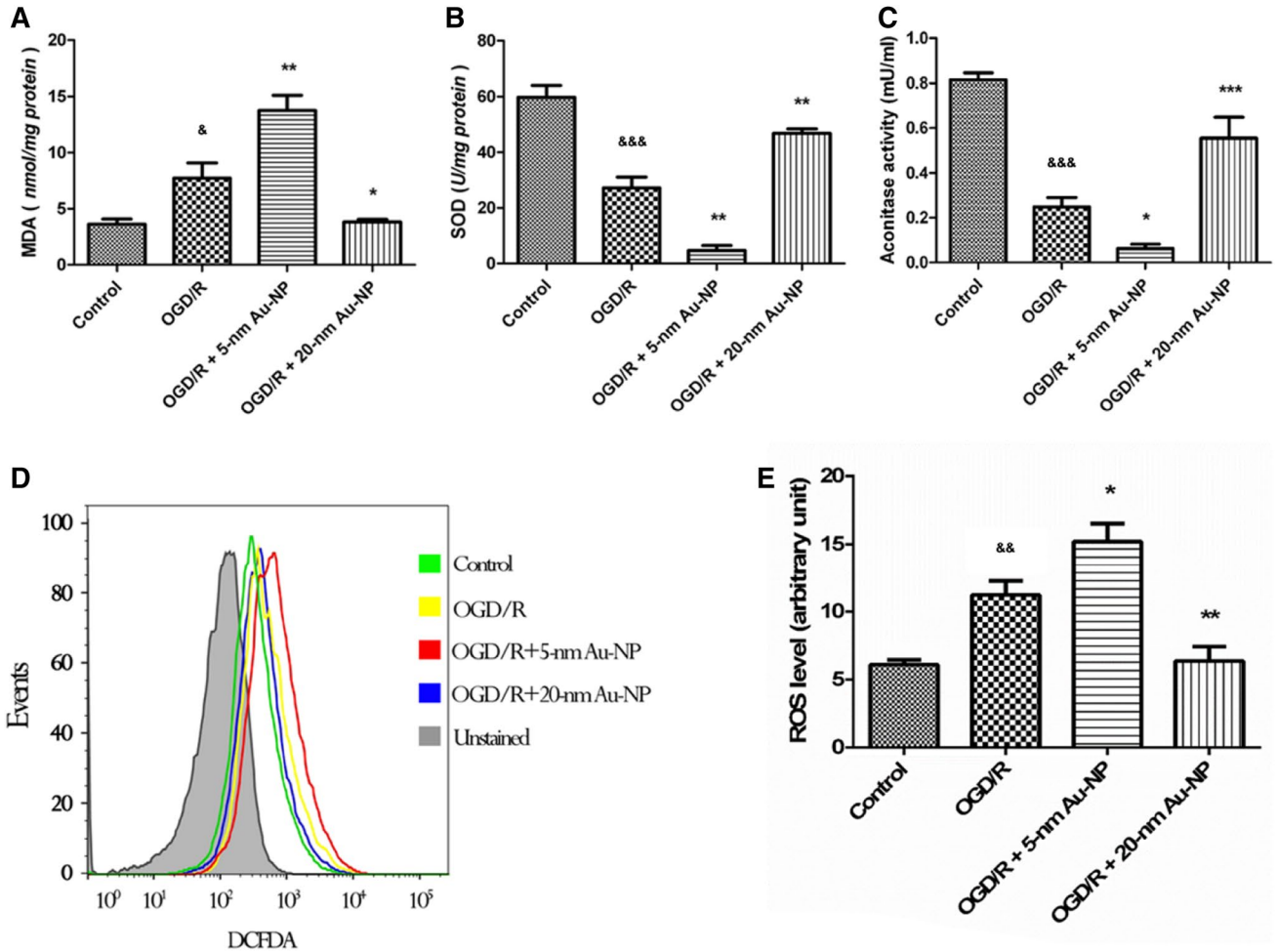

Fig. 8 Effects of Au-NPs on cellular oxidative stress. **a** Measurement of lipid peroxidation by malondialdehyde (MDA). **b** Measurement of superoxide dismutase (SOD) generation. **c** Measurement of aconitase activity. **d**, **e** A histogram of reactive oxygen species levels was derived from 2',7'-dichlorodihydrofluorescein diacetate (DCFH-DA) oxidation and quantified by flow cytometry. The results are expressed as the mean ± standard error of the mean from at least triplicate independent experiments. $^{\&}P < 0.05$ versus the control group, $^{\&\&}P < 0.01$ versus the control group, $^{\&\&\&}P < 0.001$ versus the control group, *P < 0.05 versus OGD/R group, **P < 0.01 versus OGD/R group, ***P < 0.001 versus OGD/R group

volumes compared to the I/R group [27]. In the present study, a cell viability assay revealed a similar phenomenon at the cellular level, namely that 20-nm Au-NPs may lead to neuroprotection [27], while opposite effects were observed with the administration of 5-nm Au-NPs, suggesting that 5-nm Au-NPs may have detrimental effects. Au-NPs have been widely studied for bio-sensing, photoimaging, *in vitro* diagnostics, targeted drug delivery, and even intrinsic treatment. Compared with the other applications, intrinsic treatment with Au-NPs is the subject of stronger research focus, particularly in the field of stroke research. Stroke treatment options are very limited because the BBB, one of the tightest barriers in the human body, restricts the crossing of large molecules into the cerebrospinal fluid. Au-NPs are able to penetrate the BBB due to their small size (less than 50 nm) which is similar to that of the cellular components of the BBB [49]. It has been previously shown that 7 days after injection Au-NPs are mainly located in the hippocampus, thalamus, hypothalamus, and cerebral cortex [50]. Because human organs are exposed to Au-NPs after injection, toxicity must be investigated while evaluating therapeutic potential.

Au-NP size has been associated with differences in biological function. Our previous study demonstrated, by histopathological and hematological studies, that 5-nm and 20-nm Au-NPs were not toxic to liver or kidney in rats [27]. Similar results have also been reported in rabbits, where no evidence of obvious acute toxicity within 24 h of administering 5-nm and 25-nm Au-NPs was found, and no specific changes were observed in any organs [51]. Additionally, Pan et al. [52] reported that 1.4-nm Au-NPs induced necrosis by oxidative stress and mitochondrial dysfunction in all the

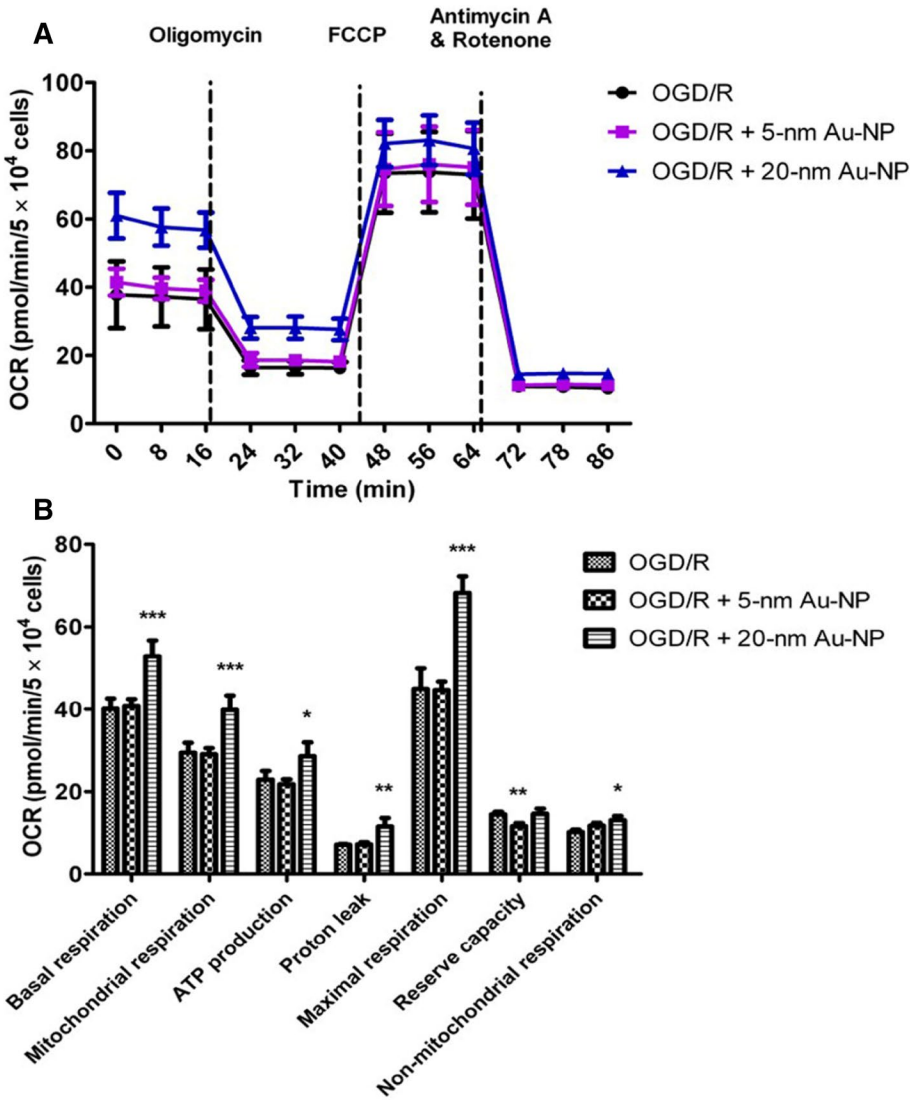

Fig. 9 Effects of Au-NPs on mitochondrial oxygen consumption. **a** Real-time measurements of oxygen consumption rate (OCR) were taken every 8 min. Agents were added every three detections in a sequence of oligomycin, FCCP, antimycin A, and rotenone. **b** Statistical analyses of all the indexes separately. The results are expressed as the mean ± standard error of the mean from at least triplicate independent experiments. *P < 0.05 versus OGD/R group, **P < 0.01 versus OGD/R group, ***P < 0.001 versus OGD/R group

cell lines examined, but they found no evidence of cellular damage when administering 15-nm Au-NPs. This result was probably due to the smaller-diameter Au-NPs being more readily accumulated into cell nuclei and organelles, thus leading to DNA damage [53–55]. This would also explain our observation that 5-nm Au-NPs exerted adverse effects on cortical neurons. Therefore, further studies should be performed to obtain a deeper understanding of the mechanisms underlying the effects of Au-NPs on cerebral I/R injury.

Neuronal apoptosis, characterized by the disruption of the MMP, concentration of the nucleus, chromatin condensation, and formation of apoptotic bodies, is a critical part of the pathogenesis of cerebral I/R injury [56, 57]. Au-NPs have been applied in cardiovascular diseases primarily as a drug carrier [58, 59], but very few studies have focused on their intrinsic effects in ischemic stroke. Rizwan et al. [33] reported that 16-nm Au-NPs could inhibit high glucose-induced apoptosis in macrophages, while our previous study suggests that anti-apoptosis may be involved in the neuroprotective effects of 20-nm Au-NPs against cerebral I/R injury [27]. The present study demonstrates that the 20-nm Au-NPs can indeed suppress neuronal apoptosis in OGD/R-exposed neurons, by increasing the MMP and deactivating cleaved caspase-3. The opposite changes in these markers were observed in OGD/R-exposed neurons treated with 5-nm Au-NPs, compared with the OGD/R group.

Oxidative stress is also a crucial factor stimulating the pathogenesis of ischemic stroke [60–62]. Numerous studies have provided substantial evidence that increased free radical formation is present in all forms of stroke injury [63, 64]. Reports have also indicated that excessive ROS production promotes cell apoptosis via lipid peroxidation, DNA lesion, and a decline in mitochondrial activity [13, 65, 66]. Several studies have proposed that Au-NPs are able to prevent oxidative stress [35, 67–69]. In this study, ROS were found to accumulate in OGD/R-exposed neurons, and 20-nm Au-NPs

were observed to reduce their production and to increase SOD activity. Conversely, 5-nm Au-NPs further increased ROS production compared to the OGD/R injury group. Altogether, these results suggest that 20-nm Au-NPs attenuate OGD/R-induced injury by suppressing oxidative stress.

According to the above observations, we propose the hypothesis that Au-NPs regulate OGD/R-induced injury via mitochondrial pathways. Mitochondria are crucial to the regulation of the central nervous system and serve to provide energy to cells by oxidative phosphorylation [70]. ROS, generated by oxidative phosphorylation, were once considered to be mere byproducts of oxidative phosphorylation, but were later found to exert many physiological and pathological functions, such as redox regulation and molecular signaling [71]. Additionally, mitochondria are also actively involved in initiating cell death. Pathological conditions can result in the opening of the mitochondrial permeability transition pore, leading to loss of mitochondrial membrane potential and triggering cell death through the necrotic or apoptotic pathways [72]. Mitochondrial dysfunction can lead to increased ROS generation, loss of ATP production, impaired calcium homeostasis, and eventually cell death [13, 73–76] and is thus considered a contributing factor to the pathological mechanisms of many neurological diseases, including stroke, Parkinson's disease, Alzheimer's disease, and major depression [77–79]. The disruption of MMP is recognized as one of the earliest events in apoptosis, and MMP is reduced under apoptotic conditions. Mitochondria can produce ATP through the electron transport chain, in which oxygen serves as an electron acceptor. In the present study, we measured basal respiration, mitochondrial respiration, ATP generation, proton leakage, maximal respiration, and reserve capacity based on the OCR. Our results indicate that 20-nm Au-NPs improve MMP depolarization and mitochondrial respiration function in rat cerebral cortical neurons after OGD/R, suggesting that 20-nm-Au-NP-induced neuroprotection is mediated by mitochondrial pathways.

Accumulative evidence has shown that Akt, an anti-apoptosis agent that phosphorylates its downstream target proteins, plays an essential role in stroke progression [80]. Apart from its influence on apoptosis, activated Akt phosphorylates GSK3β, thereby inactivating it and leading to a potent suppression of the proinflammatory response [81]. Our results suggest that p-Akt and p-GSK3β protein expression was reduced in the OGD/R group, while 20-nm Au-NPs could increase p-Akt and p-GSK3β expression after OGD/R injury. These findings suggest that the Akt/GSK3β pathway plays an important role in the neuroprotective effects of 20-nm Au-NPs on OGD/R injury.

The above findings suggest that suitably sized Au-NPs could act on neurons as biocompatible agents and may lead to promising strategies for treating I/R injury in ischemic stroke patients. Moreover, our study reveals a novel mechanism underlying the protective action of Au-NPs on primary cortical neurons against OGD/R injury. We believe that further insights into these effects may enable a deeper understanding and application of Au-NPs.

However, some limitations of this study should be noted. First, neurons were only exposed to Au-NPs for 48 h. In future studies, we hope to investigate more time points. Second, to our knowledge, this is the first report demonstrating the potent protective effects of Au-NPs on the mitochondria of primary cortical neurons exposed to OGD/R. Therefore, our hypothesis awaits further experimental confirmation, and future studies are required to explore the signaling pathways involved in the effects of Au-NPs on cortical neuronal mitochondria.

Conclusion

We demonstrated that 20-nm Au-NPs have protective effects on primary cortical neurons against OGD/R injury by supressing apoptosis and oxidative stress, and upregulating Akt/GSK3β signaling and mitochondrial pathways. These results are consistent with those of our previous *in vivo* study. Our observations have the potential to enrich the application extent of Au-NPs, and we hope that this work will establish Au-NPs as a novel and useful candidate for both basic research and clinical development of ischemic stroke therapies.

Acknowledgements This work was supported by Grants from the National Science Foundation of China (Nos. 81300999, 81470501, 81770440, and 81471783).

Compliance with Ethical Standards

Conflict of interest The authors report no conflict of interest in this work.

References

1. Benjamin EJ, Virani SS, Callaway CW, Chang AR, Cheng S, Chiuve SE, Cushman M, Delling FN, Deo R, de Ferranti SD, Ferguson JF, Fornage M, Gillespie C, Isasi CR, Jimenez MC, Jordan LC, Judd SE, Lackland D, Lichtman JH, Lisabeth L, Liu S, Longenecker CT, Lutsey PL, Matchar DB, Matsushita K, Mussolino ME, Nasir K, O'Flaherty M, Palaniappan LP, Pandey DK, Reeves MJ, Ritchey MD, Rodriguez CJ, Roth GA, Rosamond WD, Sampson UKA, Satou GM, Shah SH, Spartano NL, Tirschwell DL, Tsao CW, Voeks JH, Willey JZ, Wilkins JT, Wu JH, Alger HM, Wong SS, Muntner P (2018) Heart disease and stroke statistics-2018 update: a report from the American Heart Association. Circulation. https://doi.org/10.1161/cir.0000000000000558
2. Hankey GJ (2017) Stroke. Lancet 389(10069):641–654. https://doi.org/10.1016/S0140-6736(16)30962-X

3. Wang P, Shao BZ, Deng Z, Chen S, Yue Z, Miao CY (2018) Autophagy in ischemic stroke. Prog Neurobiol. https://doi.org/10.1016/j.pneurobio.2018.01.001
4. Feigin VL, Norrving B, Mensah GA (2017) Global burden of stroke. Circ Res 120(3):439–448. https://doi.org/10.1161/CIRCRESAHA.116.308413
5. DALYs GBD, Collaborators H, Murray CJ, Barber RM, Foreman KJ, Abbasoglu Ozgoren A, Abd-Allah F, Abera SF, Aboyans V, Abraham JP, Abubakar I, Abu-Raddad LJ, Abu-Rmeileh NM, Achoki T, Ackerman IN, Ademi Z, Adou AK, Adsuar JC, Afshin A, Agardh EE, Alam SS, Alasfoor D, Albittar MI, Alegretti MA, Alemu ZA, Alfonso-Cristancho R, Alhabib S, Ali R, Alla F, Allebeck P, Almazroa MA, Alsharif U, Alvarez E, Alvis-Guzman N, Amare AT, Ameh EA, Amini H, Ammar W, Anderson HR, Anderson BO, Antonio CA, Anwari P, Arnlov J, Arsic Arsenijevic VS, Artaman A, Asghar RJ, Assadi R, Atkins LS, Avila MA, Awuah B, Bachman VF, Badawi A, Bahit MC, Balakrishnan K, Banerjee A, Barker-Collo SL, Barquera S, Barregard L, Barrero LH, Basu A, Basu S, Basulaiman MO, Beardsley J, Bedi N, Beghi E, Bekele T, Bell ML, Benjet C, Bennett DA, Bensenor IM, Benzian H, Bernabe E, Bertozzi-Villa A, Beyene TJ, Bhala N, Bhalla A, Bhutta ZA, Bienhoff K, Bikbov B, Biryukov S, Blore JD, Blosser CD, Blyth FM, Bohensky MA, Bolliger IW, Bora Basara B, Bornstein NM, Bose D, Boufous S, Bourne RR, Boyers LN, Brainin M, Brayne CE, Brazinova A, Breitborde NJ, Brenner H, Briggs AD, Brooks PM, Brown JC, Brugha TS, Buchbinder R, Buckle GC, Budke CM, Bulchis A, Bulloch AG, Campos-Nonato IR, Carabin H, Carapetis JR, Cardenas R, Carpenter DO, Caso V, Castaneda-Orjuela CA, Castro RE, Catala-Lopez F, Cavalleri F, Cavlin A, Chadha VK, Chang JC, Charlson FJ, Chen H, Chen W, Chiang PP, Chimed-Ochir O, Chowdhury R, Christensen H, Christophi CA, Cirillo M, Coates MM, Coffeng LE, Coggeshall MS, Colistro V, Colquhoun SM, Cooke GS, Cooper C, Cooper LT, Coppola LM, Cortinovis M, Criqui MH, Crump JA, Cuevas-Nasu L, Danawi H, Dandona L, Dandona R, Dansereau E, Dargan PI, Davey G, Davis A, Davitoiu DV, Dayama A, De Leo D, Degenhardt L, Del Pozo-Cruz B, Dellavalle RP, Deribe K, Derrett S, Des Jarlais DC, Dessalegn M, Dharmaratne SD, Dherani MK, Diaz-Torne C, Dicker D, Ding EL, Dokova K, Dorsey ER, Driscoll TR, Duan L, Duber HC, Ebel BE, Edmond KM, Elshrek YM, Endres M, Ermakov SP, Erskine HE, Eshrati B, Esteghamati A, Estep K, Faraon EJ, Farzadfar F, Fay DF, Feigin VL, Felson DT, Fereshtehnejad SM, Fernandes JG, Ferrari AJ, Fitzmaurice C, Flaxman AD, Fleming TD, Foigt N, Forouzanfar MH, Fowkes FG, Paleo UF, Franklin RC, Furst T, Gabbe B, Gaffikin L, Gankpe FG, Geleijnse JM, Gessner BD, Gething P, Gibney KB, Giroud M, Giussani G, Gomez Dantes H, Gona P, Gonzalez-Medina D, Gosselin RA, Gotay CC, Goto A, Gouda HN, Graetz N, Gugnani HC, Gupta R, Gupta R, Gutierrez RA, Haagsma J, Hafezi-Nejad N, Hagan H, Halasa YA, Hamadeh RR, Hamavid H, Hammami M, Hancock J, Hankey GJ, Hansen GM, Hao Y, Harb HL, Haro JM, Havmoeller R, Hay SI, Hay RJ, Heredia-Pi IB, Heuton KR, Heydarpour P, Higashi H, Hijar M, Hoek HW, Hoffman HJ, Hosgood HD, Hossain M, Hotez PJ, Hoy DG, Hsairi M, Hu G, Huang C, Huang JJ, Husseini A, Huynh C, Iannarone ML, Iburg KM, Innos K, Inoue M, Islami F, Jacobsen KH, Jarvis DL, Jassal SK, Jee SH, Jeemon P, Jensen PN, Jha V, Jiang G, Jiang Y, Jonas JB, Juel K, Kan H, Karch A, Karema CK, Karimkhani C, Karthikeyan G, Kassebaum NJ, Kaul A, Kawakami N, Kazanjan K, Kemp AH, Kengne AP, Keren A, Khader YS, Khalifa SE, Khan EA, Khan G, Khang YH, Kieling C, Kim D, Kim S, Kim Y, Kinfu Y, Kinge JM, Kivipelto M, Knibbs LD, Knudsen AK, Kokubo Y, Kosen S, Krishnaswami S, Kuate Defo B, Kucuk Bicer B, Kuipers EJ, Kulkarni C, Kulkarni VS, Kumar GA, Kyu HH, Lai T, Lalloo R, Lallukka T, Lam H, Lan Q, Lansingh VC, Larsson A, Lawrynowicz AE, Leasher JL, Leigh J, Leung R, Levitz CE, Li B, Li Y, Li Y, Lim SS, Lind M, Lipshultz SE, Liu S, Liu Y, Lloyd BK, Lofgren KT, Logroscino G, Looker KJ, Lortet-Tieulent J, Lotufo PA, Lozano R, Lucas RM, Lunevicius R, Lyons RA, Ma S, Macintyre MF, Mackay MT, Majdan M, Malekzadeh R, Marcenes W, Margolis DJ, Margono C, Marzan MB, Masci JR, Mashal MT, Matzopoulos R, Mayosi BM, Mazorodze TT, McGill NW, McGrath JJ, McKee M, McLain A, Meaney PA, Medina C, Mehndiratta MM, Mekonnen W, Melaku YA, Meltzer M, Memish ZA, Mensah GA, Meretoja A, Mhimbira FA, Micha R, Miller TR, Mills EJ, Mitchell PB, Mock CN, Mohamed Ibrahim N, Mohammad KA, Mokdad AH, Mola GL, Monasta L, Montanez Hernandez JC, Montico M, Montine TJ, Mooney MD, Moore AR, Moradi-Lakeh M, Moran AE, Mori R, Moschandreas J, Moturi WN, Moyer ML, Mozaffarian D, Msemburi WT, Mueller UO, Mukaigawara M, Mullany EC, Murdoch ME, Murray J, Murthy KS, Naghavi M, Naheed A, Naidoo KS, Naldi L, Nand D, Nangia V, Narayan KM, Nejjari C, Neupane SP, Newton CR, Ng M, Ngalesoni FN, Nguyen G, Nisar MI, Nolte S, Norheim OF, Norman RE, Norrving B, Nyakarahuka L, Oh IH, Ohkubo T, Ohno SL, Olusanya BO, Opio JN, Ortblad K, Ortiz A, Pain AW, Pandian JD, Panelo CI, Papachristou C, Park EK, Park JH, Patten SB, Patton GC, Paul VK, Pavlin BI, Pearce N, Pereira DM, Perez-Padilla R, Perez-Ruiz F, Perico N, Pervaiz A, Pesudovs K, Peterson CB, Petzold M, Phillips MR, Phillips BK, Phillips DE, Piel FB, Plass D, Poenaru D, Polinder S, Pope D, Popova S, Poulton RG, Pourmalek F, Prabhakaran D, Prasad NM, Pullan RL, Qato DM, Quistberg DA, Rafay A, Rahimi K, Rahman SU, Raju M, Rana SM, Razavi H, Reddy KS, Refaat A, Remuzzi G, Resnikoff S, Ribeiro AL, Richardson L, Richardus JH, Roberts DA, Rojas-Rueda D, Ronfani L, Roth GA, Rothenbacher D, Rothstein DH, Rowley JT, Roy N, Ruhago GM, Saeedi MY, Saha S, Sahraian MA, Sampson UK, Sanabria JR, Sandar L, Santos IS, Satpathy M, Sawhney M, Scarborough P, Schneider IJ, Schottker B, Schumacher AE, Schwebel DC, Scott JG, Seedat S, Sepanlou SG, Serina PT, Servan-Mori EE, Shackelford KA, Shaheen A, Shahraz S, Shamah Levy T, Shangguan S, She J, Sheikhbahaei S, Shi P, Shibuya K, Shinohara Y, Shiri R, Shishani K, Shiue I, Shrime MG, Sigfusdottir ID, Silberberg DH, Simard EP, Sindi S, Singh A, Singh JA, Singh L, Skirbekk V, Slepak EL, Sliwa K, Soneji S, Soreide K, Soshnikov S, Sposato LA, Sreeramareddy CT, Stanaway JD, Stathopoulou V, Stein DJ, Stein MB, Steiner C, Steiner TJ, Stevens A, Stewart A, Stovner LJ, Stroumpoulis K, Sunguya BF, Swaminathan S, Swaroop M, Sykes BL, Tabb KM, Takahashi K, Tandon N, Tanne D, Tanner M, Tavakkoli M, Taylor HR, Te Ao BJ, Tediosi F, Temesgen AM, Templin T, Ten Have M, Tenkorang EY, Terkawi AS, Thomson B, Thorne-Lyman AL, Thrift AG, Thurston GD, Tillmann T, Tonelli M, Topouzis F, Toyoshima H, Traebert J, Tran BX, Trillini M, Truelsen T, Tsilimbaris M, Tuzcu EM, Uchendu US, Ukwaja KN, Undurraga EA, Uzun SB, Van Brakel WH, Van De Vijver S, van Gool CH, Van Os J, Vasankari TJ, Venketasubramanian N, Violante FS, Vlassov VV, Vollset SE, Wagner GR, Wagner J, Waller SG, Wan X, Wang H, Wang J, Wang L, Warouw TS, Weichenthal S, Weiderpass E, Weintraub RG, Wenzhi W, Werdecker A, Westerman R, Whiteford HA, Wilkinson JD, Williams TN, Wolfe CD, Wolock TM, Woolf AD, Wulf S, Wurtz B, Xu G, Yan LL, Yano Y, Ye P, Yentur GK, Yip P, Yonemoto N, Yoon SJ, Younis MZ, Yu C, Zaki ME, Zhao Y, Zheng Y, Zonies D, Zou X, Salomon JA, Lopez AD, Vos T (2015) Global, regional, and national disability-adjusted life years (DALYs) for 306 diseases and injuries and healthy life expectancy (HALE) for 188 countries, 1990-2013: quantifying the epidemiological transition. Lancet 386(10009):2145–2191. https://doi.org/10.1016/s0140-6736(15)61340-x
6. Kisler K, Nelson AR, Montagne A, Zlokovic BV (2017) Cerebral blood flow regulation and neurovascular dysfunction in Alzheimer disease. Nat Rev Neurosci 18(7):419–434. https://doi.org/10.1038/nrn.2017.48

7. Goyal M, Demchuk AM, Menon BK, Eesa M, Rempel JL, Thornton J, Roy D, Jovin TG, Willinsky RA, Sapkota BL, Dowlatshahi D, Frei DF, Kamal NR, Montanera WJ, Poppe AY, Ryckborst KJ, Silver FL, Shuaib A, Tampieri D, Williams D, Bang OY, Baxter BW, Burns PA, Choe H, Heo JH, Holmstedt CA, Jankowitz B, Kelly M, Linares G, Mandzia JL, Shankar J, Sohn SI, Swartz RH, Barber PA, Coutts SB, Smith EE, Morrish WF, Weill A, Subramaniam S, Mitha AP, Wong JH, Lowerison MW, Sajobi TT, Hill MD, Investigators ET (2015) Randomized assessment of rapid endovascular treatment of ischemic stroke. N Engl J Med 372(11):1019–1030. https://doi.org/10.1056/NEJMoa1414905
8. Attwell D, Buchan AM, Charpak S, Lauritzen M, Macvicar BA, Newman EA (2010) Glial and neuronal control of brain blood flow. Nature 468(7321):232–243. https://doi.org/10.1038/nature09613
9. Zlokovic BV (2011) Neurovascular pathways to neurodegeneration in Alzheimer's disease and other disorders. Nat Rev Neurosci 12(12):723–738. https://doi.org/10.1038/nrn3114
10. Venkat P, Chopp M, Chen J (2017) Blood-brain barrier disruption, vascular impairment, and ischemia/reperfusion damage in diabetic stroke. J Am Heart Assoc. https://doi.org/10.1161/jaha.117.005819
11. Iadecola C (2013) The pathobiology of vascular dementia. Neuron 80(4):844–866. https://doi.org/10.1016/j.neuron.2013.10.008
12. Duehrkop C, Rieben R (2014) Ischemia/reperfusion injury: effect of simultaneous inhibition of plasma cascade systems versus specific complement inhibition. Biochem Pharmacol 88(1):12–22. https://doi.org/10.1016/j.bcp.2013.12.013
13. Wang M, Sun GB, Zhang JY, Luo Y, Yu YL, Xu XD, Meng XB, Zhang MD, Lin WB, Sun XB (2015) Elatoside C protects the heart from ischaemia/reperfusion injury through the modulation of oxidative stress and intracellular Ca(2)(+) homeostasis. Int J Cardiol 185:167–176. https://doi.org/10.1016/j.ijcard.2015.03.140
14. At Groehler, Kren S, Li Q, Robledo-Villafane M, Schmidt J, Garry M, Tretyakova N (2018) Oxidative cross-linking of proteins to DNA following ischemia-reperfusion injury. Free Radic Biol Med. https://doi.org/10.1016/j.freeradbiomed.2018.03.010
15. Koeppen M, Lee JW, Seo SW, Brodsky KS, Kreth S, Yang IV, Buttrick PM, Eckle T, Eltzschig HK (2018) Hypoxia-inducible factor 2-alpha-dependent induction of amphiregulin dampens myocardial ischemia-reperfusion injury. Nat Commun 9(1):816. https://doi.org/10.1038/s41467-018-03105-2
16. Li Y, Liu X (2018) Novel insights into the role of mitochondrial fusion and fission in cardiomyocyte apoptosis induced by ischemia/reperfusion. J Cell Physiol. https://doi.org/10.1002/jcp.26522
17. Xu H, Qin W, Hu X, Mu S, Zhu J, Lu W, Luo Y (2018) Lentivirus-mediated overexpression of OTULIN ameliorates microglia activation and neuroinflammation by depressing the activation of the NF-kappaB signaling pathway in cerebral ischemia/reperfusion rats. J Neuroinflamm 15(1):83. https://doi.org/10.1186/s12974-018-1117-5
18. Moussaddy A, Demchuk AM, Hill MD (2018) Thrombolytic therapies for ischemic stroke: Triumphs and future challenges. Neuropharmacology. https://doi.org/10.1016/j.neuropharm.2017.11.010
19. Dreaden EC, Alkilany AM, Huang X, Murphy CJ, El-Sayed MA (2012) The golden age: gold nanoparticles for biomedicine. Chem Soc Rev 41(7):2740–2779. https://doi.org/10.1039/c1cs15237h
20. Nicolardi S, van der Burgt YEM, Codee JDC, Wuhrer M, Hokke CH, Chiodo F (2017) Structural characterization of biofunctionalized gold nanoparticles by ultrahigh-resolution mass spectrometry. ACS Nano 11(8):8257–8264. https://doi.org/10.1021/acsnano.7b03402
21. Tan G, Onur MA (2018) Cellular localization and biological effects of 20 nm-gold nanoparticles. J Biomed Mater Res, Part A 106(6):1708–1721. https://doi.org/10.1002/jbm.a.36373
22. Zong J, Cobb SL, Cameron NR (2017) Peptide-functionalized gold nanoparticles: versatile biomaterials for diagnostic and therapeutic applications. Biomater Sci 5(5):872–886. https://doi.org/10.1039/c7bm00006e
23. Vilela P, Heuer-Jungemann A, El-Sagheer A, Brown T, Muskens OL, Smyth NR, Kanaras AG (2018) Sensing of vimentin mRNA in 2D and 3D models of wounded skin using DNA-coated gold nanoparticles. Small. https://doi.org/10.1002/smll.201703489
24. Saraiva C, Praca C, Ferreira R, Santos T, Ferreira L, Bernardino L (2016) Nanoparticle-mediated brain drug delivery: overcoming blood-brain barrier to treat neurodegenerative diseases. J Controlled Release 235:34–47. https://doi.org/10.1016/j.jconrel.2016.05.044
25. Dykman L, Khlebtsov N (2012) Gold nanoparticles in biomedical applications: recent advances and perspectives. Chem Soc Rev 41(6):2256–2282. https://doi.org/10.1039/c1cs15166e
26. Betzer O, Perets N, Angel A, Motiei M, Sadan T, Yadid G, Offen D, Popovtzer R (2017) In vivo neuroimaging of exosomes using gold nanoparticles. ACS Nano 11(11):10883–10893. https://doi.org/10.1021/acsnano.7b04495
27. Liu Z, Shen Y, Wu Y, Yang Y, Wu J, Zhou P, Lu X, Guo Z (2013) An intrinsic therapy of gold nanoparticles in focal cerebral ischemia-reperfusion injury in rats. J Biomed Nanotechnol 9(6):1017–1028
28. Paula MM, Petronilho F, Vuolo F, Ferreira GK, De Costa L, Santos GP, Effting PS, Dal-Pizzol F, Dal-Bo AG, Frizon TE, Silveira PC, Pinho RA (2015) Gold nanoparticles and/or N-acetylcysteine mediate carrageenan-induced inflammation and oxidative stress in a concentration-dependent manner. J Biomed Mater Res, Part A 103(10):3323–3330. https://doi.org/10.1002/jbm.a.35469
29. Jeon KI, Byun MS, Jue DM (2003) Gold compound auranofin inhibits IkappaB kinase (IKK) by modifying Cys-179 of IKK-beta subunit. Exp Mol Med 35(2):61–66. https://doi.org/10.1038/emm.2003.9
30. Fernandez TD, Pearson JR, Leal MP, Torres MJ, Blanca M, Mayorga C, Le Guevel X (2015) Intracellular accumulation and immunological properties of fluorescent gold nanoclusters in human dendritic cells. Biomaterials 43:1–12. https://doi.org/10.1016/j.biomaterials.2014.11.045
31. Barathmanikanth S, Kalishwaralal K, Sriram M, Pandian SR, Youn HS, Eom S, Gurunathan S (2010) Anti-oxidant effect of gold nanoparticles restrains hyperglycemic conditions in diabetic mice. J Nanobiotechnol 8:16. https://doi.org/10.1186/1477-3155-8-16
32. Gao N, Sun H, Dong K, Ren J, Qu X (2015) Gold-nanoparticle-based multifunctional amyloid-beta inhibitor against Alzheimer's disease. Chemistry 21(2):829–835. https://doi.org/10.1002/chem.201404562
33. Rizwan H, Mohanta J, Si S, Pal A (2017) Gold nanoparticles reduce high glucose-induced oxidative-nitrosative stress regulated inflammation and apoptosis via tuberin-mTOR/NF-kappaB pathways in macrophages. Int J Nanomed 12:5841–5862. https://doi.org/10.2147/IJN.S141839
34. Ferreira GK, Cardoso E, Vuolo FS, Michels M, Zanoni ET, Carvalho-Silva M, Gomes LM, Dal-Pizzol F, Rezin GT, Streck EL, Paula MM (2015) Gold nanoparticles alter parameters of oxidative stress and energy metabolism in organs of adult rats. Biochem Cell Biol 93(6):548–557. https://doi.org/10.1139/bcb-2015-0030
35. Muller AP, Ferreira GK, Pires AJ, de Bem Silveira G, de Souza DL, Brandolfi JA, de Souza CT, Paula MMS, Silveira PCL (2017) Gold nanoparticles prevent cognitive deficits, oxidative stress and inflammation in a rat model of sporadic dementia of Alzheimer's type. Mater Sci Eng C Mater Biol Appl 77:476–483. https://doi.org/10.1016/j.msec.2017.03.283

36. Zorov DB, Filburn CR, Klotz LO, Zweier JL, Sollott SJ (2000) Reactive oxygen species (ROS)-induced ROS release: a new phenomenon accompanying induction of the mitochondrial permeability transition in cardiac myocytes. J Exp Med 192(7):1001–1014
37. Love JC, Estroff LA, Kriebel JK, Nuzzo RG, Whitesides GM (2005) Self-assembled monolayers of thiolates on metals as a form of nanotechnology. Chem Rev 105(4):1103–1169. https://doi.org/10.1021/cr0300789
38. Daniel MC, Astruc D (2004) Gold nanoparticles: assembly, supramolecular chemistry, quantum-size-related properties, and applications toward biology, catalysis, and nanotechnology. Chem Rev 104(1):293–346. https://doi.org/10.1021/cr030698+
39. Kuttner C, Mayer M, Dulle M, Moscoso AI, Lopez-Romero JM, Forster S, Fery A, Perez-Juste J, Contreras-Caceres R (2018) Seeded growth synthesis of gold nanotriangles: size control, SAXS analysis, and SERS performance. ACS Appl Mater Interfaces. https://doi.org/10.1021/acsami.7b19081
40. Guo C, Wang S, Duan J, Jia N, Zhu Y, Ding Y, Guan Y, Wei G, Yin Y, Xi M, Wen A (2017) Protocatechualdehyde protects against cerebral ischemia-reperfusion-induced oxidative injury via protein kinase cepsilon/Nrf2/HO-1 pathway. Mol Neurobiol 54(2):833–845. https://doi.org/10.1007/s12035-016-9690-z
41. Liu Z, Wu Y, Guo Z, Liu Y, Shen Y, Zhou P, Lu X (2014) Effects of internalized gold nanoparticles with respect to cytotoxicity and invasion activity in lung cancer cells. PLoS ONE 9(6):e99175. https://doi.org/10.1371/journal.pone.0099175
42. Zhao K, Hao H, Liu J, Tong C, Cheng Y, Xie Z, Zang L, Mu Y, Han W (2015) Bone marrow-derived mesenchymal stem cells ameliorate chronic high glucose-induced beta-cell injury through modulation of autophagy. Cell Death Dis 6:e1885. https://doi.org/10.1038/cddis.2015.230
43. Zhang C, Shi S (2018) Physiological and proteomic responses of contrasting alfalfa (*Medicago sativa* L.) varieties to PEG-induced osmotic stress. Front Plant Sci 9:242. https://doi.org/10.3389/fpls.2018.00242
44. Wu L, Guo X, Hartson SD, Davis MA, He H, Medeiros DM, Wang W, Clarke SL, Lucas EA, Smith BJ, von Lintig J, Lin D (2017) Lack of beta, beta-carotene-9', 10'-oxygenase 2 leads to hepatic mitochondrial dysfunction and cellular oxidative stress in mice. Mol Nutr Food Res. https://doi.org/10.1002/mnfr.201600576
45. Dranka BP, Benavides GA, Diers AR, Giordano S, Zelickson BR, Reily C, Zou L, Chatham JC, Hill BG, Zhang J, Landar A, Darley-Usmar VM (2011) Assessing bioenergetic function in response to oxidative stress by metabolic profiling. Free Radic Biol Med 51(9):1621–1635. https://doi.org/10.1016/j.freeradbiomed.2011.08.005
46. Dranka BP, Zielonka J, Kanthasamy AG, Kalyanaraman B (2012) Alterations in bioenergetic function induced by Parkinson's disease mimetic compounds: lack of correlation with superoxide generation. J Neurochem 122(5):941–951. https://doi.org/10.1111/j.1471-4159.2012.07836.x
47. Kang H, Lee GH, Jung H, Lee JW, Nam Y (2018) Inkjet-printed biofunctional thermo-plasmonic interfaces for patterned neuromodulation. ACS Nano 12(2):1128–1138. https://doi.org/10.1021/acsnano.7b06617
48. Brand MD, Nicholls DG (2011) Assessing mitochondrial dysfunction in cells. Biochem J 435(2):297–312. https://doi.org/10.1042/BJ20110162
49. Shilo M, Motiei M, Hana P, Popovtzer R (2014) Transport of nanoparticles through the blood-brain barrier for imaging and therapeutic applications. Nanoscale 6(4):2146–2152. https://doi.org/10.1039/c3nr04878k
50. Sousa F, Mandal S, Garrovo C, Astolfo A, Bonifacio A, Latawiec D, Menk RH, Arfelli F, Huewel S, Legname G, Galla HJ, Krol S (2010) Functionalized gold nanoparticles: a detailed in vivo multimodal microscopic brain distribution study. Nanoscale 2(12):2826–2834. https://doi.org/10.1039/c0nr00345j
51. Glazer ES, Zhu C, Hamir AN, Borne A, Thompson CS, Curley SA (2011) Biodistribution and acute toxicity of naked gold nanoparticles in a rabbit hepatic tumor model. Nanotoxicology 5(4):459–468. https://doi.org/10.3109/17435390.2010.516026
52. Pan Y, Leifert A, Ruau D, Neuss S, Bornemann J, Schmid G, Brandau W, Simon U, Jahnen-Dechent W (2009) Gold nanoparticles of diameter 1.4 nm trigger necrosis by oxidative stress and mitochondrial damage. Small 5(18):2067–2076. https://doi.org/10.1002/smll.200900466
53. Paino IM, Marangoni VS, de Oliveira Rde C, Antunes LM, Zucolotto V (2012) Cyto and genotoxicity of gold nanoparticles in human hepatocellular carcinoma and peripheral blood mononuclear cells. Toxicol Lett 215(2):119–125. https://doi.org/10.1016/j.toxlet.2012.09.025
54. Lopez-Chaves C, Soto-Alvaredo J, Montes-Bayon M, Bettmer J, Llopis J, Sanchez-Gonzalez C (2018) Gold nanoparticles: distribution, bioaccumulation and toxicity. In vitro and in vivo studies. Nanomedicine 14(1):1–12. https://doi.org/10.1016/j.nano.2017.08.011
55. Xia Q, Li H, Liu Y, Zhang S, Feng Q, Xiao K (2017) The effect of particle size on the genotoxicity of gold nanoparticles. J Biomed Mater Res, Part A 105(3):710–719. https://doi.org/10.1002/jbm.a.35944
56. Takemura G, Kanoh M, Minatoguchi S, Fujiwara H (2013) Cardiomyocyte apoptosis in the failing heart—a critical review from definition and classification of cell death. Int J Cardiol 167(6):2373–2386. https://doi.org/10.1016/j.ijcard.2013.01.163
57. Caccamo A, Branca C, Piras IS, Ferreira E, Huentelman MJ, Liang WS, Readhead B, Dudley JT, Spangenberg EE, Green KN, Belfiore R, Winslow W, Oddo S (2017) Necroptosis activation in Alzheimer's disease. Nat Neurosci 20(9):1236–1246. https://doi.org/10.1038/nn.4608
58. Ho YT, Poinard B, Kah JC (2016) Nanoparticle drug delivery systems and their use in cardiac tissue therapy. Nanomedicine 11(6):693–714. https://doi.org/10.2217/nnm.16.6
59. Bharadwaj VN, Nguyen DT, Kodibagkar VD, Stabenfeldt SE (2018) Nanoparticle-based therapeutics for brain injury. Adv Healthc Mater. https://doi.org/10.1002/adhm.201700668
60. Chamorro A, Dirnagl U, Urra X, Planas AM (2016) Neuroprotection in acute stroke: targeting excitotoxicity, oxidative and nitrosative stress, and inflammation. Lancet Neurol 15(8):869–881. https://doi.org/10.1016/S1474-4422(16)00114-9
61. Zhao H, Han Z, Ji X, Luo Y (2016) Epigenetic regulation of oxidative stress in ischemic stroke. Aging Dis 7(3):295–306. https://doi.org/10.14336/AD.2015.1009
62. Cheng YC, Sheen JM, Hu WL, Hung YC (2017) Polyphenols and oxidative stress in atherosclerosis-related ischemic heart disease and stroke. Oxid Med Cell longev 2017:8526438. https://doi.org/10.1155/2017/8526438
63. Suh SW, Shin BS, Ma H, Van Hoecke M, Brennan AM, Yenari MA, Swanson RA (2008) Glucose and NADPH oxidase drive neuronal superoxide formation in stroke. Ann Neurol 64(6):654–663. https://doi.org/10.1002/ana.21511
64. Li P, Stetler RA, Leak RK, Shi Y, Li Y, Yu W, Bennett MVL, Chen J (2017) Oxidative stress and DNA damage after cerebral ischemia: potential therapeutic targets to repair the genome and improve stroke recovery. Neuropharmacology. https://doi.org/10.1016/j.neuropharm.2017.11.011
65. Halestrap AP (2009) What is the mitochondrial permeability transition pore? J Mol Cell Cardiol 46(6):821–831. https://doi.org/10.1016/j.yjmcc.2009.02.021
66. Yoshitomi T, Nagasaki Y (2014) Reactive oxygen species-scavenging nanomedicines for the treatment of oxidative stress

injuries. Adv Healthc Mater 3(8):1149–1161. https://doi.org/10.1002/adhm.201300576
67. Dkhil MA, Bauomy AA, Diab MS, Al-Quraishy S (2015) Antioxidant and hepatoprotective role of gold nanoparticles against murine hepatic schistosomiasis. Int J Nanomed 10:7467–7475. https://doi.org/10.2147/IJN.S97622
68. Lai TH, Chung CH, Chen BH, Hung CF, Inbaraj BS, Ma MC, Chen HM, Tsou CJ, Wu PH, Wu WB (2016) Gold nanoparticles compromise TNF-alpha-induced endothelial cell adhesion molecule expression through NF-kappaB and protein degradation pathways and reduce neointima formation in a rat carotid balloon injury model. J Biomed Nanotechnol 12(12):2185–2201
69. Ferreira GK, Cardoso E, Vuolo FS, Galant LS, Michels M, Goncalves CL, Rezin GT, Dal-Pizzol F, Benavides R, Alonso-Nunez G, Andrade VM, Streck EL, da Silva Paula MM (2017) Effect of acute and long-term administration of gold nanoparticles on biochemical parameters in rat brain. Mater Sci Eng, C 79:748–755. https://doi.org/10.1016/j.msec.2017.05.110
70. Chan DC (2006) Mitochondria: dynamic organelles in disease, aging, and development. Cell 125(7):1241–1252. https://doi.org/10.1016/j.cell.2006.06.010
71. Zhou B, Tian R (2018) Mitochondrial dysfunction in pathophysiology of heart failure. J Clin Investig. https://doi.org/10.1172/jci120849
72. Bernardi P, Di Lisa F (2015) The mitochondrial permeability transition pore: molecular nature and role as a target in cardioprotection. J Mol Cell Cardiol 78:100–106. https://doi.org/10.1016/j.yjmcc.2014.09.023
73. Schapira AH (2007) Mitochondrial dysfunction in Parkinson's disease. Cell Death Differ 14(7):1261–1266. https://doi.org/10.1038/sj.cdd.4402160
74. Vosler PS, Graham SH, Wechsler LR, Chen J (2009) Mitochondrial targets for stroke: focusing basic science research toward development of clinically translatable therapeutics. Stroke 40(9):3149–3155. https://doi.org/10.1161/STROKEAHA.108.543769
75. Schon EA, Przedborski S (2011) Mitochondria: the next (neurode) generation. Neuron 70(6):1033–1053. https://doi.org/10.1016/j.neuron.2011.06.003
76. Dawson TM, Dawson VL (2017) Mitochondrial mechanisms of neuronal cell death: potential therapeutics. Annu Rev Pharmacol Toxicol 57:437–454. https://doi.org/10.1146/annurev-pharmtox-010716-105001
77. Czarny P, Wigner P, Galecki P, Sliwinski T (2018) The interplay between inflammation, oxidative stress, DNA damage, DNA repair and mitochondrial dysfunction in depression. Prog Neuropsychopharmacol Biol Psychiatry 80(Pt C):309–321. https://doi.org/10.1016/j.pnpbp.2017.06.036
78. Dixit S, Fessel JP, Harrison FE (2017) Mitochondrial dysfunction in the APP/PSEN1 mouse model of Alzheimer's disease and a novel protective role for ascorbate. Free Radic Biol Med 112:515–523. https://doi.org/10.1016/j.freeradbiomed.2017.08.021
79. Zhang X, Du L, Zhang W, Yang Y, Zhou Q, Du G (2017) Therapeutic effects of baicalein on rotenone-induced Parkinson's disease through protecting mitochondrial function and biogenesis. Sci Rep 7(1):9968. https://doi.org/10.1038/s41598-017-07442-y
80. Li M, Feng B, Wang L, Guo S, Zhang P, Gong J, Zhang Y, Zheng A, Li H (2015) Tollip is a critical mediator of cerebral ischaemia-reperfusion injury. J Pathol 237(2):249–262. https://doi.org/10.1002/path.4565
81. Martin M, Rehani K, Jope RS, Michalek SM (2005) Toll-like receptor-mediated cytokine production is differentially regulated by glycogen synthase kinase 3. Nat Immunol 6(8):777–784. https://doi.org/10.1038/ni1221